Aggregated residential multi-carrier energy storage as voltage control provider in low-voltage distribution networks

Alpízar-Castillo, Joel; Ramírez-Elizondo, Laura; van Voorden, Arjan; Bauer, Pavol

DOI
10.1016/j.est.2025.117507

Publication date
2025

Document Version
Final published version

Published in
Journal of Energy Storage

Journal of Energy Storage 132 (2025) 117507

Contents lists available at ScienceDirect

Journal of Energy Storage

journal homepage: www.elsevier.com/locate/est

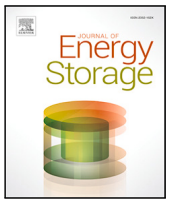

Research papers

Aggregated residential multi-carrier energy storage as voltage control provider in low-voltage distribution networks

Joel Alpízar-Castillo [a,*], Laura Ramírez-Elizondo [a], Arjan van Voorden [a,b], Pavol Bauer [a]

[a] DCE&S group, Delft University of Technology, Mekelweg 6, Delft, 2628CD, Zuid Holland, The Netherlands
[b] Stedin Group, Blaak 8, Rotterdam, 3011 TA, Zuid Holland, The Netherlands

ARTICLE INFO

Keywords:
Aggregation
Low-voltage distribution network
Multi-carrier energy system
Voltage control

ABSTRACT

The inclusion of PV and heat pumps in residential low-voltage distribution systems is a fundamental component of the energy transition. Nevertheless, adoptions below 40% can already cause voltage conditions incompliant with the standard EN50160 during winter. Aggregated storage systems have been proposed as a solution; however, the literature generally assumes full observability and controllability of the assets, which is unrealistic in many cases. This paper evaluates the potential of aggregated single- and multi-carrier storage systems to maintain voltage stability in low voltage networks, considering separated controllers for the prosumer and the aggregator. We used a real 301-node residential distribution network in the Netherlands as case study. Our results demonstrate that aggregated multi-carrier energy storage can ensure the voltage conditions established in the standard EN50160 for energy transition adoptions up to 80%, while aggregated single-carrier storage can reach 60% and centralized storage only 40%. We concluded that aggregation of storage assets increases the utilization of the existing grid infrastructure, reducing reinforcement costs for the DSOs. However, the energy storage assets' high investment costs lead to unattractive conditions for single- and multi-carrier storage, compared to a case with only PV and heat pumps. Considering the current market conditions, using storage for voltage support would require economic compensations. These findings provide DSOs valuable insight on alternative solutions to grid reinforcement and centralized storage to address the challenges of the energy transition.

1. Introduction

Traditionally, medium- and high-voltage networks have been the centre of attention of system operators, as high-power systems are normally connected to such systems. Such connections require detailed planning, and system operators usually demand some degree of flexibility from asset owners, either consumers or generators. In such a scheme, residential low-voltage distribution networks were considered to be less risky. They only consume energy with relatively low power individual loads, since the most energy-intensive activities (transportation and heating) relied on fossil fuels. Nevertheless, the energy transition dramatically shifted the paradigm for residential consumers.

In the energy transition scheme, residential prosumers are encouraged to install distributed generators based on renewable energy sources (RES), typically PV systems, to address the fossil-fuel dependence of the energy supply chain [1]. In addition, many existing households are replacing their gas boilers with heat pumps (HP), which are also becoming the norm for new buildings [2]. Similarly, the electrification of transportation has reached a point where the purchase of electric vehicles (EVs) now competes with internal combustion, and the number houses installing chargers soared [3]. This way, distribution system operators (DSOs) have seen a drastic change in the power exchange behaviour from residential consumers in a short time, challenging their traditional reinforcement-based system management strategies.

The responses from DSOs can be categorized into regulatory and policy, and technical. The first includes administrative actions requested by the DSO to the regulatory authorities to minimize the effect of the energy transition in the electrical network. For example, in Germany and the United Kingdom there is a limit to how much power a residential system can inject into the grid, based on its nominal power [4,5]. Also, some authors have demonstrated that flat energy and variable demand tariffs are less risky while still being attractive for prosumers [6]. The second category includes technical actions so that the cyber–physical distribution system can manage the new power flow conditions. Among those actions are grid reinforcement and more

* Corresponding author.
E-mail address: J.J.AlpizarCastillo@tudelft.nl (J. Alpízar-Castillo).

https://doi.org/10.1016/j.est.2025.117507
Received 10 March 2025; Received in revised form 27 May 2025; Accepted 18 June 2025
Available online 12 July 2025

Nomenclature

(k)	Current timestep
$(k \pm i)$	ith timestep

Abbreviations

BESS	Battery energy storage system
DRES	Distributed renewable energy sources
DSO	Distribution system operators
EMS	Energy management systems
EMS	Home energy management systems
EV	Electric vehicle
HP	Heat pump
MCES	Multi-carrier energy system
PV	Photovoltaic
TESS	Thermal energy storage System

Variables

β	GA population
Δt	Time between time steps
δ	Specific policy
$\dot{m}$	Mass flow
$\dot{Q}$	Thermal power
η	Efficiency
λ	Energy cost
π	General policy
ρ	Density
A	Area
C	Cost function
c	Specific thermal capacity
E	Electric energy
G	Solar irradiance
m	Mass
P	Electric power
Q	Thermal energy
q	Airflow
T	Temperature
t	GA generation
U	Total heat transfer coefficient
COP	Coefficient of performance

robust power flow control mechanisms [7]. Those categories, despite fundamentally different, share one common bottleneck, both require long realization times; the former due to regulatory, social acceptance and institutional barriers, and the second due to required technological development, engineering design and commissioning [8] and, more recently, a shortage in workforce [9]. This way, effective solutions require using available technologies and the current regulatory frameworks as much as possible.

1.1. Relevant literature

There is plenty of literature available about models used to maximize profit when participating in the energy market. In general, this profit is either from energy arbitrage, or providing ancillary services [10]. Although some authors classify energy arbitrage as an ancillary service, as prices are set to incentivize certain consumption patterns to indirectly support the grid, we will classify them separately in this work. Participating in the existing ancillary services markets requires the prosumer to follow a set of rules [11], and is limited to medium and high voltage networks, with large-scale assets. However, there are no major market constraints to profit based on energy arbitrage, once the interconnection limit is defined, and it can be done at any voltage level. Particularly at low-voltage networks, most DSOs cannot enforce power limitations on prosumers, either passively by setting a cap below the contracted power, or actively by sending signals in real-time for prosumers to adjust their power. For this reason, algorithms used to profit using residential assets (e.g., EVs or HPs) focus on this mechanism, considering day-ahead pricing [12].

A model predictive control strategy was used by [13] to control a residential PV-BESS (battery energy storage system) system, reducing energy costs up to 30% compared to a mean nonlinear model predictive control. The same system architecture was approached using the long short-term memory algorithm by [14] to predict generation and consumption patterns, achieving good accuracy. More complex system architectures, forming multi-carrier systems, have also been studied. For example, in [12], a system including PV, solar collectors, BESS, EV, thermal energy storage (TESS) and heat pumps was optimized to minimize the cost of energy purchase and the ageing of the BESS, achieving a reduction of 20% to 45% when compared to state-of-the-art solutions, but highlighting the high computational cost. Similarly, the work in [15] used max–min game theory to control the power flow of a system comprised of a PV, a BESS, 30 EV chargers and a hydrogen fuel cell-electrolyzer installed in a five-floor office building to minimize the degradation of the BESS and the hydrogen system. The results surpassed EMSs using mixed-integer linear programming and heuristic methods in reducing the degradation between 12.64% and 75.61% for the BESS and 23.16% and 82.81% for the fuel cell, respectively. Homer Pro was used by [16] to optimally size a microgrid comprised of a centralized wind, PV, biomass and BESS system, minimizing the net present cost for a case study using the load of the Putrajaya city in Malaysia, reaching an overall energy cost of 0.118 $/kWh.

The previous mechanisms can be done without causing major problems in the distribution grid if the number of participants is low enough. Nonetheless, in higher adoption levels (i.e., higher number of prosumers in the grid), they pose a risk to the network [6,17]; thus, aggregation control is required [18]. Aggregation can be either set to support the local network where the assets are connected or the upstream network through the substation. For instance, [19] proved that aggregating assets in lower voltage networks can create load profiles at the substation, so that the aggregator can participate in the ancillary services market on behalf of all the individual members using the IEEE 33-node test network. This is particularly attractive for medium- and high-voltage operators, as the power and voltage problems at the substation can be addressed. Still, keeping the limits at the substation does not guarantee that power or voltage limitations in the conductors and nodes downstream are fulfilled.

To address conductor overloading, the literature offers some strategies used to coordinate the prosumers. Mixed integer linear programming and heuristic methods are compared by [20] in the IEEE 13-node and 123-node networks to control BESS to minimize the effect of DRES in distribution networks. Using the mixed integer linear programming reduced the degradation of the BESS by 34%. A two-stage distributionally robust optimization model is used by [21] to minimize the cost of energy storage investment and distribution network operation under extreme conditions for a PV-BESS system. The method was tested using the IEEE 33-node network and PV and loads from a distribution network in China, resulting in better PV accommodation capacity and resilience of the distribution network while minimizing costs, when compared to stochastic optimization and robust optimization approaches. In [22], the same test network was used, used to minimize voltage variations when combining PV and BESS, improving the maximum node offset by 4.4%.

The method proposed by [23] identifies and evaluates flexibility perimeters in radial distribution networks. Two case studies using the IEEE 123-node network with different voltage load areas demonstrating

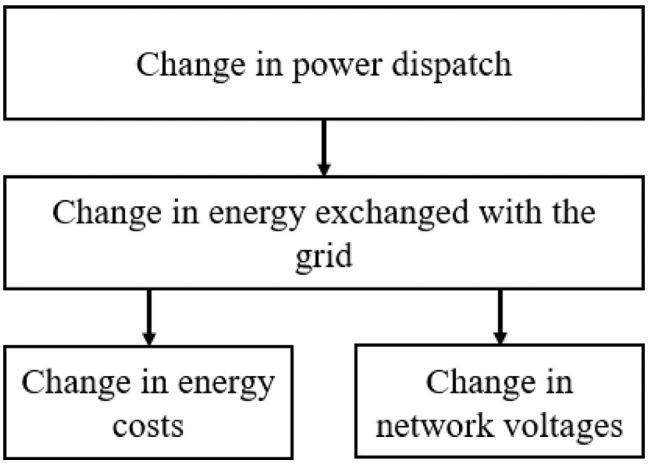

Fig. 1. Causality sequence considered for the analysis.

that increasing the number of areas decreases the flexibility volume required for voltage control. A weighted multi-objective optimization to minimize power loss and voltage deviations in the lines, energy cost and PV energy curtailed was done in [24]. Their results suggest that adjusting the optimization weights can maintain the voltage within limits in a 15-node medium voltage distribution network in Yangzhou, China, with controlled PV, BESS and EVs. Likewise, [25] used a convex approximation of the exact nonlinear programming model to minimize the energy costs and power losses in the lines for a representative urban case using the IEEE 33-node network, and a rural case using a 27-node network. The results showed an improvement of around 1.5% compared to continuous genetic algorithm, particle swarm optimization and parallel vortex search algorithm, but computation time was reduced up to one order of magnitude.

As a response to the complexity of building the network model, a model-free controller was proposed in [26] to keep voltage variations in the 1 ± 0.05 pu range using PV and synchronous generator assets. The test in a medium voltage 21-node distribution network demonstrated correction times in the order of seconds. Alternatively, [27] uses an effective grid load limit as indicator for grid stability, controlling it using a maximum load threshold and a ramp rate limit to avoid sudden changes in the load. When comparing a user centric and a grid centric control strategy, the grid centric control showed better peak mitigation, reaching an utilization factor of 51.4%, whereas the user centric control reached 48.6%. In [28], an EV charging profile was converted into an equivalent model using Homer, connected to a PV, a battery and a diesel generator systems. The results showed a 76.69% reduction in grid dependency for the EV charge.

1.2. Contributions

Based on the literature review, the gaps found include:

- control techniques for single-carrier systems, focusing on mid- to large-scale assets in medium voltage distribution networks, leaving aside multi-carrier systems and low-voltage residential distribution networks,
- dependency on test networks with a small number of connections (either DRES and BESS assets, or loads) for case scenarios, instead of using data from existing distribution networks,
- aggregators are assumed to have full observability and control over the assets, potentially causing privacy challenges for residential prosumers who would own assets connected to the network, and
- the control is usually either consumer-centred or DSO-centred, instead of relating one to another.

Therefore, considering a real low-voltage distribution network in the Netherlands as case scenario, the contributions of this work are:

1. evaluating the effect of different adoption levels of four different single- and multi-carrier system architectures in residential buildings in low-voltage distribution networks, as the existing literature has focused on single-carrier systems on medium- and high-voltage networks,
2. assessing the flexibility potential of aggregated multi-carrier systems, comprised of a PV, HP, BESS and TESS systems, in residential buildings, compared to a centralized single-carrier PV-BESS system, and
3. analysing the trade-off between economic cost and flexibility of a residential multi-carrier energy system for three different aggregation schemes, considering separated control for the prosumer and aggregator, in contrast with the DSO-centric approach of most of the literature.

To realize those contributions, the analysis done follows the flow presented in Fig. 1. To understand the changes in energy cost for prosumers and voltages in the low-voltage network, we performed an analysis on the grid exchange behaviour caused by the change in internal power dispatch at the household level for different single- and multi-carrier systems.

2. Mathematical descriptions

2.1. Distribution networks

A model of a low-voltage distribution network is required to evaluate the aggregation strategy. In this case, we used a voltage-based model, as residential loads are unlikely to cause major frequency shifts. The network's topology is then represented as an admittance matrix A, the voltages at every node as a vector V_n, and the impedances and currents between two interconnected nodes are Z and I, respectively. This power-flow problem is solved using an iterative method, following

$$V_n(k+1) = A\,V_n(k) - Z(k)\;I(k) + B\,V_0(k)\;, \tag{1}$$

where V_0 is the voltage inputs at the substations and B is a matrix indicating to which nodes they are connected. Note that during the iteration process, it is assumed that the values for the impedances, currents and feeder voltage are constants, as the iterative process is done every time step k. The current estimation has a similar approach, following

$$I(k+1) = A^{\mathrm{T}}\,I(k) + I_n(k)\;, \tag{2}$$

where I_n is a vector with the current at every node. The current, however, is also a function of the voltage, as

$$I_n(k) = \frac{S_n(k)}{V_n(k)} \tag{3}$$

where S_n is the apparent power at every node [20]. Fig. 2 shows the method used to solve the network's power-flow.

2.2. Multi-carrier energy system

Some buildings in the network were coupled with one or more devices to create different scenarios, as will be described in Section 3. This gradual inclusion of devices provides information on the individual effect at the network level. The more complex system couples all the considered devices into a multi-carrier energy system (MCES) comprised of a PV, a battery energy storage system, a heat pump and an underground thermal energy storage system. The models for each device were taken from [29], and a summary of the models is provided in Table 1. For the Li-ion battery, we followed the semi-empirical degradation model proposed in [30] to account for calendar

Table 1
Equations used to model the components of the MCES.

Parameter	Symbol	Equation	
PV generation	$P_{PV}(k)$	$= A_{PV} G(k) \eta_{STC} \left(1 - \beta \left[T_{PV}(k-1) - T_{ref}\right]\right)$	(6)
BESS energy	$E_{BESS}(k)$	$= \begin{cases} E_{BESS}(k-1) + \eta^{c}_{BESS} P_{BESS}(k-1)\Delta t - E^{SD}(k-1) & \forall\, P_{BESS}(k-1) < 0 \\ E_{BESS}(k-1) + \frac{P_{BESS}(k-1)}{\eta^{d}_{BESS}}\Delta t - E^{SD}(k-1) & \forall\, P_{BESS}(k-1) > 0 \end{cases}$	(7)
TESS power	$\dot{Q}_{TESS}(k)$	$= \eta_{TESS} \dot{m}_f c_f \left[T_{sup} - T_{TESS}(k-1)\right]$	(8)
TESS temperature	$T_{TESS}(k)$	$= T_{TESS}(k-1) + \frac{\Delta t \left[\eta^{c}_{TESS} \dot{Q}^{TESS}_{HP}(k-1) - \frac{\dot{Q}_{TESS}(k-1)}{\eta^{d}_{TESS}} + \dot{Q}^{SD}(k-1)\right]}{m\, c}$	(9)
HP COP	COP(k)	$= 7.90471 e^{-0.024\left[T_{ret}(k-1) - T_{amb}(k-1)\right]}$	(10)
HP thermal power	$\dot{Q}_{HP}(k)$	$= \eta_{HP} \dot{m}_f c_f \left[T_{sup} - T_{ret}(k-1)\right]$	(11)
Thermal demand	$\dot{Q}_D(k)$	$= \left(\sum_{i=1}^{n} U_i A_i + c_a \rho_a q_v + c_a \rho_a q_i\right) \left[T_{in}(k-1) - T_{out}(k-1)\right]$	(12)
Indoor temperature	$T_{in}(k)$	$= T_{in}(k-1) + \frac{\Delta t \left[\dot{Q}_{TESS}(k-1) + \dot{Q}_{HP}(k-1) - \dot{Q}_D(k-1)\right]}{\sum_{i=1}^{n} m_i c_i}$	(13)
Return temperature	$T_{ret}(k)$	$= T_{ret}(k-1) + \frac{\dot{Q}_{TESS}(k-1) + \dot{Q}_{HP}(k-1) - \dot{Q}_D(k-1)}{\dot{m}_f c_f}$	(14)

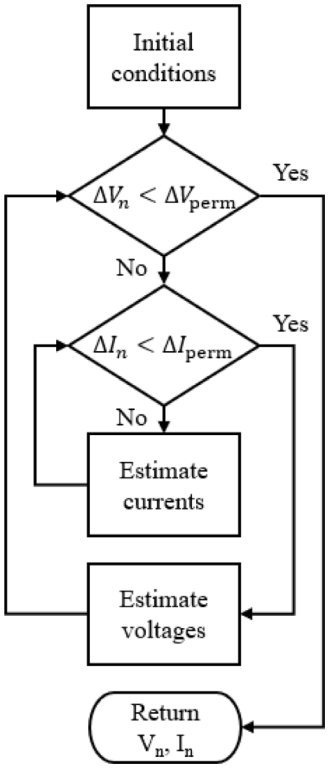

Fig. 2. Flow diagram used to estimate the nodes' voltage and current.

and cycling ageing. The thermal energy storage is an underground, well-mixed water tank with separated charge and discharge coils. The heat loss to the environment of both the TESS and the house was modelled following the methods proposed in [29]. The distribution of the thermal power in the house is done using a water system that can use the TESS and the HP individually or simultaneously. The HP is used to charge the tank.

The PV systems used per house are sized to reach as close as possible to a net-zero energy building, using 400 W modules, with an area A_{PV} of 2 m^2, efficiency at standard test conditions η_{STC} of 18.4%, temperature coefficient β of −0.3%/°C. The BESS charge and discharge efficiencies are set at 94.3%, with a maximum permitted power of ±10 kW and a capacity of 10 kWh. The TESS is assumed to be filled with 4 m^3 of water, and the heat exchangers have an efficiency η_{TESS} and η_{HP} of 80% with a mass flow of $\dot{m}_f$ of 0.22 m^3/s through the heating circuit. The supply temperature of the network T_{sup} is 50 °C. The details of the thermal losses can be found in [29].

2.3. Local EMS control

For this work, we propose thermal comfort, represented as the deviation from a setpoint temperature, energy purchase costs under a day-ahead pricing scheme, and the deviation from a power exchange setpoint defined by an aggregator as objectives. These policies are recalculated for each time step k, The thermal comfort policy δ^T defines whether the HP and the TESS should be available to heat the house or not, thus $\delta^T = [\delta^T_{HP}, \delta^T_{TESS}]$, with

$$\delta^T_{HP} = \begin{cases} 0, & \forall \quad T_{set} \le T_{in} \\ 1, & \forall \quad T_{set} > T_{in} \end{cases}, \tag{4}$$

and

$$\delta^T_{TESS} = \begin{cases} 0, & \forall \quad T_{set} \le T_{in} \\ 1, & \forall \quad T_{set} > T_{in} \end{cases}. \tag{5}$$

The energy purchase cost policy $\delta^\lambda = [\delta^\lambda_{HP}, \delta^\lambda_{TESS}, \delta^\lambda_{HP\,\to\,TESS}, \delta^{HP}_{HP\to TESS}, \delta^{SoC}_{HP\to TESS}, \delta^{SoC}_{TESS}]$ suggests which heating device should be used at any given point k, based on the energy price λ reported in the day-ahead list. To define the prices as high or low and thus increase or decrease the power exchanged with the grid, we calculated the distribution quartiles of the DA prices. We defined as *low prices* those included in the first quartile, i.e., below λ_{Q25}. Therefore, the policy for the activation of the heat pump to heat the house is

$$\delta^\lambda_{HP} = \begin{cases} 1, & \forall \quad \lambda \le \lambda_{Q25} \\ 0, & \forall \quad \lambda > \lambda_{Q25} \end{cases}, \tag{15}$$

the policy for the discharge of the TESS is

$$\delta^\lambda_{TESS} = \begin{cases} 0, & \forall \quad \lambda \le \lambda_{Q25} \\ 1, & \forall \quad \lambda > \lambda_{Q25} \end{cases}, \tag{16}$$

and the policy for charging the TESS is

$$\delta^\lambda_{HP\to TESS} = \begin{cases} 1, & \forall \quad \lambda \le \lambda_{Q25} \\ 0, & \forall \quad \lambda > \lambda_{Q25} \end{cases}. \tag{17}$$

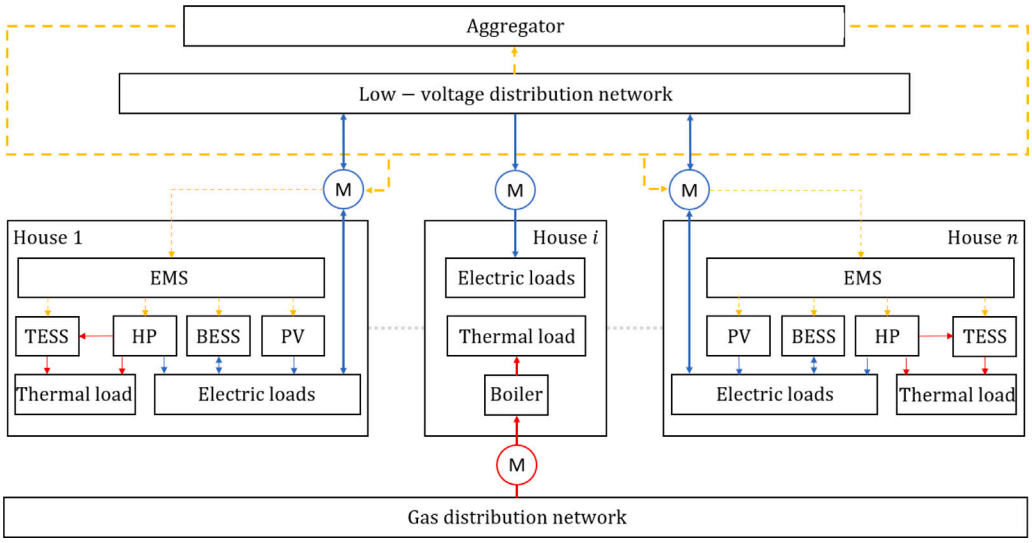

Fig. 3. Control scheme representing the interactions between the aggregator, the low-voltage distribution network, the consumers and the prosumers (the yellow lines represent communication flow, the blue lines electric power flow, and the red lines thermal power flow). (For interpretation of the references to colour in this figure legend, the reader is referred to the web version of this article.)

Also, as the HP cannot heat the house and charge the TESS simultaneously, thus

$$\delta^{HP}_{\mathrm{HP}\to\mathrm{TESS}} = \begin{cases} 1\,, & \forall \quad \delta_{\mathrm{HP}} = 0 \\ 0\,, & \forall \quad \delta_{\mathrm{HP}} = 1 \end{cases}. \tag{18}$$

Then, to account for the SoC constraints of the TESS, we considered

$$\delta^{\mathrm{SoC}}_{\mathrm{HP}\to\mathrm{TESS}} = \begin{cases} 1\,, & \forall \quad T_{\mathrm{TESS}} < T^{\max}_{\mathrm{TESS}} \\ 0\,, & \forall \quad T_{\mathrm{TESS}} \geq T^{\max}_{\mathrm{TESS}} \end{cases} \tag{19}$$

for the charge, and

$$\delta^{\mathrm{SoC}}_{\mathrm{TESS}} = \begin{cases} 1\,, & \forall \quad T^{\min}_{\mathrm{TESS}} \leq T_{\mathrm{TESS}} \\ 0\,, & \forall \quad T^{\min}_{\mathrm{TESS}} > T_{\mathrm{TESS}} \end{cases} \tag{20}$$

for the discharge.

Finally, the power from the PV and BESS depend on the grid exchange setpoint P^* defined by the aggregator. To minimize the degradation of the BESS and curtailment on the PV, the policy $\delta^{\mathrm{P}} = [P_{\mathrm{BESS}}, P_{\mathrm{PV}}]$ prioritizes using as much power from the PV as possible. However, unlike the TESS, where its primary controller regulates the flow so that the output temperature reaches the supply temperature (which is a fixed value), the policy for the BESS defines its power – delivered or consumed, – which is limited by its current state-of-charge and the available PV power. The power boundaries for the BESS are

$$\overline{P}^{\mathrm{perm}}_{\mathrm{BESS}} = \begin{cases} P^{\max}_{\mathrm{BESS}}\,, & \forall \quad P_{\mathrm{BESS}} \geq P^{\max}_{\mathrm{BESS}} \\ C_{\mathrm{BESS}} \Delta SoC^{\max}_{\mathrm{BESS}}\,, & \forall \quad P_{\mathrm{BESS}} < P^{\max}_{\mathrm{BESS}} \end{cases} \tag{21}$$

for the maximum and

$$\underline{P}^{\mathrm{perm}}_{\mathrm{BESS}} = \begin{cases} C_{\mathrm{BESS}} \Delta SoC^{\min}_{\mathrm{BESS}}\,, & \forall \quad P_{\mathrm{BESS}} > -P^{\max}_{\mathrm{BESS}} \\ -P^{\max}_{\mathrm{BESS}}\,, & \forall \quad P_{\mathrm{BESS}} \leq -P^{\max}_{\mathrm{BESS}} \end{cases} \tag{22}$$

for the minimum power, with

$$\Delta SoC^{\max}_{\mathrm{BESS}} = \frac{SoC_{\mathrm{BESS}} - SoC^{\min}_{\mathrm{BESS}}}{\Delta t} \tag{23}$$

and

$$\Delta SoC^{\min}_{\mathrm{BESS}} = \frac{SoC_{\mathrm{BESS}} - SoC^{\max}_{\mathrm{BESS}}}{\Delta t}\,, \tag{24}$$

as provided in [31]. Then, the boundaries for the BESS, based on the available PV power are

$$\overline{P}^{\mathrm{set}}_{\mathrm{BESS}} = P_L + P_{\mathrm{HP}} + + P_{\mathrm{HP}\to\mathrm{TESS}} - P^{\mathrm{av}}_{\mathrm{PV}} - P^* \tag{25}$$

and

$$\underline{P}^{\mathrm{set}}_{\mathrm{BESS}} = P_L + P_{\mathrm{HP}} + P_{\mathrm{HP}\to\mathrm{TESS}} - P^*\,, \tag{26}$$

Thus, the policies for the PV and BESS are, respectively,

$$P_{\mathrm{BESS}} = \begin{cases} \underline{P}^{\mathrm{set}}_{\mathrm{BESS}}\,, & \forall \quad \left(\underline{P}^{\mathrm{set}}_{\mathrm{BESS}} \geq \underline{P}^{\mathrm{perm}}_{\mathrm{BESS}}\right) \wedge \left(\underline{P}^{\mathrm{set}}_{\mathrm{BESS}} \leq \overline{P}^{\mathrm{perm}}_{\mathrm{BESS}}\right) \\ \underline{P}^{\mathrm{perm}}_{\mathrm{BESS}}\,, & \forall \quad \left(\underline{P}^{\mathrm{set}}_{\mathrm{BESS}} \leq \underline{P}^{\mathrm{perm}}_{\mathrm{BESS}}\right) \wedge \left(\overline{P}^{\mathrm{set}}_{\mathrm{BESS}} \geq \underline{P}^{\mathrm{perm}}_{\mathrm{BESS}}\right) \\ \overline{P}^{\mathrm{perm}}_{\mathrm{BESS}}\,, & \forall \quad \underline{P}^{\mathrm{set}}_{\mathrm{BESS}} \geq \overline{P}^{\mathrm{perm}}_{\mathrm{BESS}} \\ \underline{P}^{\mathrm{perm}}_{\mathrm{BESS}}\,, & \text{else} \end{cases} \tag{27}$$

and

$$P_{\mathrm{PV}} = \begin{cases} P^{\mathrm{av}}_{\mathrm{PV}}\,, & \forall \quad \left(\underline{P}^{\mathrm{set}}_{\mathrm{BESS}} \geq \underline{P}^{\mathrm{perm}}_{\mathrm{BESS}}\right) \wedge \left(\underline{P}^{\mathrm{set}}_{\mathrm{BESS}} \leq \overline{P}^{\mathrm{perm}}_{\mathrm{BESS}}\right) \\ \underline{P}^{\mathrm{perm}}_{\mathrm{BESS}} - \underline{P}^{\mathrm{set}}_{\mathrm{BESS}}\,, & \forall \quad \left(\underline{P}^{\mathrm{set}}_{\mathrm{BESS}} \leq \underline{P}^{\mathrm{perm}}_{\mathrm{BESS}}\right) \wedge \left(\overline{P}^{\mathrm{set}}_{\mathrm{BESS}} \geq \underline{P}^{\mathrm{perm}}_{\mathrm{BESS}}\right) \\ 0\,, & \forall \quad \underline{P}^{\mathrm{set}}_{\mathrm{BESS}} \geq \overline{P}^{\mathrm{perm}}_{\mathrm{BESS}} \\ P^{\mathrm{av}}_{\mathrm{PV}}\,, & \text{else} \end{cases} \tag{28}$$

prioritizing meeting the thermal load for two reasons: first, thermal comfort is deemed more important than charging the TESS. Second, and perhaps less obvious, the HP's coefficient of performance is higher when heating the house than when charging the TESS due to the required supply temperatures. Therefore, prioritizing the thermal load will also reduce the purchase from the grid.

The general policy π_k for each timestep k is then comprised of the individual policies per device j and objective i, resulting in

$$\pi_k = [\delta^T, \delta^\lambda, \delta^P] \tag{29}$$

thus, for each device, the control policy is given by

$$\delta_j = \prod_{\delta^i \in \pi_k} \delta^i_j\,, \tag{30}$$

2.4. Aggregation control

It is expected that increasing the number of assets in the grid will lead to congestion, in particular, if they use the same EMS, which

follows the energy price. For this reason, we implemented an aggregator, so that the effect on the network is minimized. Unlike most aggregators in the literature that are assumed to have full observability over the assets at each node, our aggregator only has information up the meter, i.e., can only measure the current and power a particular node exchanges with the grid, and the voltage at every node in the network. This way, the aggregator would provide a setpoint power to each prosumer, and the local EMS would handle the power allocation to fulfil such a setpoint (see Fig. 3). Consumers (i.e., households without flexibility assets) are excluded from the setpoint assignment. These conditions, of course, create challenges for the control strategy in terms of asset controllability, but in the view of the authors, provide a more realistic approach in terms of short-term implementation and data privacy management.

Since the aggregator has no visibility on what are the states of the assets behind the meter, it is assumed that the power exchanged with the grid at any point k is the optimal value found by the local EMS. Based on this assumption, we propose to find the power setpoints P^* for every prosumer while minimizing the change between the measured power and the actual setpoint. This way, the optimization problem is formulated as

$$\min_{P_i^*} \quad \sum_{i \in N} \left(P_i^* - P_i\right)^2 \tag{31}$$

$$s.t. \quad P_i^* = P_i \,, \forall\, i \in N_c \,, \tag{32a}$$

$$P_i^* = 0 \,, \forall\, i \in N_d \,. \tag{32b}$$

$$V_{\min} \leq V_i \leq V_{\max} \,, \forall\, i \in N \,, \tag{32c}$$

where, i is the node number, the set N contains all the nodes in the network, N_c is the subset with the nodes where a consumer is connected to the grid, and N_d the subset with the distribution nodes where no loads are connected. The capacity of the conductors was not included in the constraints as it was not observed to cause problems. Note that, as shown in Section 2.4, the process to calculate V_i is iterative, which might interfere with the optimization process. For that reason, we propose using an approximation for the worst voltage in the grid (worst defined as the node whose voltage is further from 1 p.u. either towards consumption or injection) as a function of the average exchanged power with the grid per node $\hat{V}(\overline{P}_{\text{Grid}})$, as will be detailed in Section 4.1. This way (32c) is replaced for

$$V_{\min} \leq \hat{V}(\overline{P}_{\text{Grid}}) \leq V_{\max} \,, \forall\, i \in N \,. \tag{33}$$

3. Scenarios description

This work aims to demonstrate the effect of different energy transition scenarios on a low-voltage residential network. The network used is a 400 V, 301-node network with 114 houses with yearly consumption information provided by the Dutch DSO Stedin. The yearly consumption of the 114 houses ranged from 500 kWh to 15 000 kWh, with an average of 3000 kWh. The distribution of energy consumption is shown in Fig. 4. As heating consumption was not provided, the houses were classified according to their consumption as a 55 m^2 apartment, a 120 m^2 apartment and a 240 m^2 house for consumptions between 0–1000 kWh, 1000–4000 kWh and above 4000 kWh, respectively.

Despite the details of the network cannot be shared, it must be noted that, as it is a low-voltage network, the reactive component of the cabling impedance is dominant. Thus, voltage control can be achieved by altering the active power, unlike medium- and high-voltage systems, whose impedances are dominated by the reactive component. Therefore, voltage control should be done through modifications in the reactive power. Similarly, detailed data on the consumption cannot be provided due to confidentiality, therefore the sizes of the PV systems cannot be provided either, as they were sized to achieve a near-zero

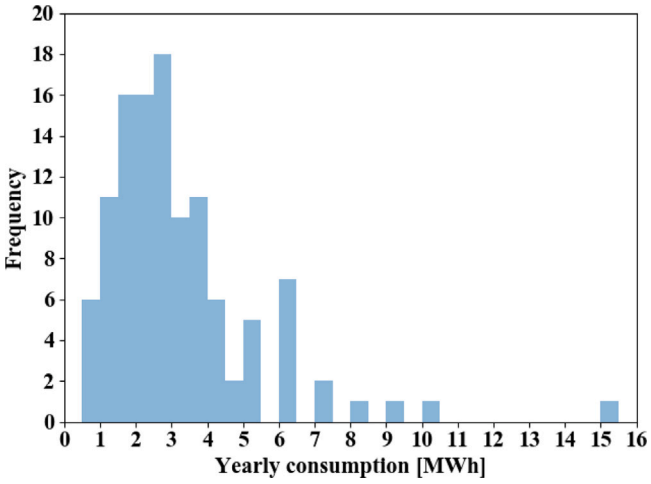

Fig. 4. Distribution of the yearly consumption per household in the network.

consumption per building. However, for all the houses, the BESS considered has 10 kW/10 kWh, and the TESS was a 200 kWh underground water tank.

For each scenario, four adoption percentages were evaluated (20%, 40%, 60% and 80%) during a week during winter (1 to 7 January) and during summer (26 June to 3 July). We considered five different random sets of nodes to locate the systems in the network for each adoption level to better represent a real case where the DSOs cannot control where new prosumers would install their systems. These sets were maintained for all the scenarios so that they could be compared.

Seven energy transition scenarios were considered. A *base case* is defined as a reference, considering only the existing electric loads and gas heating. Then, the *RES inclusion* was considered in the form of PV systems sized for near-net-zero houses. *Heating electrification* through heat pumps is added to eliminate the dependency on gas boilers in the selected nodes. Battery storage systems were added to create a *single-carrier non-aggregated storage* system, as these batteries are not communicating with each other, and a *single-carrier aggregated storage* system where an aggregator sends setpoints to the prosumers, who would follow them if possible. A *multi-carrier non-aggregated storage* scenario was then created by adding thermal energy storage to the previous scenario. With this architecture, two more scenarios were constructed, a *multi-carrier aggregated storage* system, where an aggregator directs the power to be exchanged with the grid at any point, and a *multi-carrier semi-aggregated storage* system, where the aggregator suggests a power setpoint, but the local EMS can decide to follow it or not, based on its own strategy. Table 2 summarizes the scenarios and the variables considered for each.

We used different metrics to compare scenarios 1 to 7 from the DSO perspective and from the prosumer perspective. For the former, we considered the voltage outside the 1 ± 0.05 p.u. ($V_{0.95}$ and $V_{1.05}$) and 1 ± 0.1 p.u. ($V_{0.90}$ and $V_{1.10}$) ranges per node. At the prosumer level, we compared for each selected house the change in the energy exchange (ΔE_G^{in} for consumption and ΔE_G^{out} for injection). Similarly, the change in the cost of electricity (ΔC_E), total energy including electricity and gas ($\Delta C_{E,g}$), the PV energy curtailed (ΔE_{PV}), the total energy consumed by the heat pump (ΔE_{HP}), the energy stored ($\Delta E_{\text{BESS}}^{\text{in}}$) and degradation ($\Delta C_{\text{BESS}}$) of the battery, the thermal energy used by the heat pump to charge the TESS ($\Delta E_{\text{PV}}^{\text{TESS}}$) and the thermal energy used by the TESS to heat the house (ΔQ_{TESS}). For the cost analysis, we considered a dynamic energy price contract based on day-ahead tariffs, as the only other energy market at the residential level would use fixed-priced energy costs; unlike higher voltage systems that allow different market mechanisms. As each adoption level has multiple cases, we provided

Table 2
Scenario description.

Scenario	Architecture	EMS objective
0: Base case	–	–
1: RES inclusion	PV	–
2: Heat electrification	PV + HP	Thermal comfort
3: Single-carrier non-aggregated storage	PV + HP + BESS	Thermal comfort + minimize costs
4: Single-carrier aggregated storage	PV + HP + BESS	Thermal comfort + grid support
5: Multi-carrier non-aggregated storage	PV + HP + BESS + TESS	Thermal comfort + minimize costs
6: Multi-carrier aggregated storage	PV + HP + BESS + TESS	Thermal comfort + grid support
7: Multi-carrier semi-aggregated storage	PV + HP + BESS + TESS	Thermal comfort + minimize costs + grid support
8: Centralized Storage[a]	PV + BESS	Grid support

[a] The centralized storage is considered to compensate for scenario 2.

the range between the minimum and maximum value among those cases per metric.

Scenario 8 will be analysed only from the DSO perspective. This is because it is intended to compensate for the prosumer's behaviour without interacting with them for scenarios 1 and 2. This way, we only consider the voltage outside the 1 ± 0.05 p.u. ($V_{0.95}$ and $V_{1.05}$) and 1 ± 0.1 p.u. ($V_{0.90}$ and $V_{1.10}$) ranges per node. However, the location and sizing of the BESS (energy and power) and PV must be determined. To define the node where the centralized system will be connected, the network will be analysed for each case per adoption to determine the most critical node, defined as the node with higher accumulated voltage deviations outside the permitted range, calculated by

$$\Sigma_{V,i} = \left[\sum_{k=0}^{T} V_{\min} - \underline{V}_i(k)\right] + \left[\sum_{k=1}^{T} \overline{V}_i(k) - V_{\max}\right], \forall \underline{V}_i(k) < V_{\min}, \overline{V}_i(k) > V_{\max}, i \in N. \quad (34)$$

Once the node is defined, a BESS and PV system was placed on that node to evaluate whether a centralized system can ensure voltage compliance with the standard EN50160.

4. Results

4.1. Voltage estimation

The iterative nature of the power flow solution method, using the node voltages in the network as constraints, might lead to high computational costs or, ultimately, unfeasibilities. For that reason, we evaluated the unaggregated scenarios to find an alternative to estimate the network behaviour. We simulated each scenario for a 100% adoption level and then plotted the minimum and maximum voltages in the network against the average grid power per node $\overline{P}_{\text{Grid}}$. As shown in Figs. 5(a), 5(c), 5(e) and 5(g), two polynomial correlation became evident for all scenarios. On the one hand, for the positive average grid powers (consumption), the worst voltage in the network is the minimum (shown in red), whereas the best voltage is the maximum (shown in blue). On the other hand, when the average grid power is negative (injection), the correlation is reversed; i.e., the worst voltage is the maximum, and the best is the minimum. This behaviour is consistent with previous studies in power systems where small incremental changes in power in the network resulted in quasi-lineal voltage behaviour [32].

Interestingly, the best and worst voltage points, despite reversing at $\overline{P}_{\text{Grid}} = 0$, complement each other. Using a second-order polynomial regression, we were able to estimate the worst voltage curve $\hat{V}$ as a function of the average grid power with very high accuracy (black line). We then repeated this experiment for 20 different combinations of node samplings and adoption levels per scenario (see Fig. 7 for details on the sampling distribution) during summer and winter without extrapolating the average grid power ranges per case, as shown in Figs. 5(b), 5(d), 5(f) and 5(h). As can be seen, there is a strong correlation between the average grid power and the worst voltage in the network, which is then confirmed plotting the yearly curves per scenario together in Fig. 6. The resulting approximation of the worst voltage on the grid that is used for (33) is

$$\hat{V}(\overline{P}_{\text{Grid}}) = -0.00083106\,\overline{P}^2_{\text{Grid}} - 0.03378\,\overline{P}_{\text{Grid}} + 0.9997 \quad (35)$$

4.2. Scenarios analysis

The analysis was carried out for a representative week during winter (1 to 7 January) and summer (26 June to 3 July), as the technical standard EN50160 requires that the voltage remain within ± 0.1 p.u. during 95% of the week. Knowing that the location of the node where the system will be placed leads to different results on the network, we created five random samples per adoption percentage, uniformly distributed throughout the network, as shown in Fig. 7. The network was simulated, including the corresponding system architecture per scenario in the selected nodes. A summary of the results is shown in Tables 3 and 4. The simulations were done using Python in a computer with a processor Intel i7-1185G7 and 16 GB of RAM. Simulating one week took between 10 and 13 minutes in total, depending on the scenario.

Starting with the voltage results shown in Tables 3 and 4, on the one hand, it can be noted that the inclusion of PV systems does not result in overvoltages beyond the regulation. Considering that the PV systems for scenario 1 and onwards were sized for a near-net-zero building using the base case as reference, the adoption required to surpass the 1.05 p.u. limit defined in the standard EN50160 is around 80% during summer. The low production during winter makes the power injection effect in the grid barely noticeable. On the other hand, it can be noticed that the inclusion of heat pumps does have a negative impact on the grid. Adoptions around 40% causes non-compliance with the 0.95 p.u. limit. Fig. 8 shows how the energy consumed from the grid changes for a typical week in winter and summer for scenarios 1, 2 and 5. Adding the PV alone reduces the overall consumption as expected; however, the inclusion of heat pumps in scenario 2 and then thermal storage in scenario 5 resulted in energy consumption up to two orders of magnitude greater than the base case, as the heating comes only from electricity. There is also a decay in the change in energy consumption proportional to the yearly consumption, but the PV can only compensate for prosumers with consumptions above 2 MWh/year during summer in scenarios 2 and 3. The reasons are discussed in Section 5.

From a cost perspective, however, the PV and the heat pump are complimentary, which can be seen in the reduction of energy export E_G^{out} into the grid in scenario 2 when compared with scenario 1. Despite the consumption of the heat pump increasing considerably the energy consumption from the grid E_G^{in} (see Fig. 8), therefore the electricity cost C_E, especially during winter, thanks to the dynamic pricing and solar generation, the overall energy cost $C_{E,g}$ (electricity plus gas) decreases for all houses, as shown in Fig. 9. Particularly during winter, Figs. 9(c) and 9(e) show that for the different types of houses (studio, apartment and detached), the change in energy cost has different slopes when adding the heat pump in scenarios 2 and 5, opposite to the smooth slope observed in the change in electricity cost. During summer, the

Table 3
Result ranges per season for different adoption levels (20%–40%).

		0%	20%							40%						
			1	2	3	4	5	6	7	1	2	3	4	5	6	7
Winter	$V_{0.95}$ [%]	3.263	3.263	3.56–3.66	3.53–3.66	3.31–3.59	5.46–8.90	3.20–3.46	3.94–8.07	3.26	6.75–7.99	6.70–7.95	3.24–3.57	24.07–25.26	3.14–3.41	22.64–24.17
	$V_{1.05}$ [%]	0	0	0	0	0	0	0	0	0	0	0	0	0	0	0
	$V_{0.90}$ [%]	0.020	0.020	0.107–0.130	0.100–0.127	0.001978–0.1360	0.235–0.298	0.00346–0.0870	0.213–0.290	0.020	0.338–0.367	0.331–0.360	0.0593–0.1276	2.98–4.47	0.0400–0.0727	1.145–2.42
	$V_{1.10}$ [%]	0	0	0	0	0	0	0	0	0	0	0	0	0	0	0
	ΔC_E [%]	*Ref*	–(5.48–6.84)	19.09–281	15.80–281.1	30.44–459.6	34.62–831	34.78–675.01	45.23–1026	–(5.35–6.71)	19.09–323	15.80–322.9	39.52–855.5	34.62–955	29.31–1041	45.23–1147
	$\Delta C_{E,g}$ [%]	*Ref*	–(5.48–6.84)	–(60.17–78.56)	–(61.27–78.56)	–(53.51–71.04)	–(45.09–65.41)	–(55.28–73.84)	–(33.81–59.03)	–(5.35–6.71)	–(60.17–78.85)	–(61.27–78.85)	–(40.33–76.73)	–(44.92–65.67)	–(42.36–73.80)	–(33.51–59.58)
	$\Delta E_{\mathbf{G}}^{\mathbf{in}}$ [%]	*Ref*	–(4.01–4.94)	59.84–665.1	25.7–665.1	80.57–1624	151.3–3295	76.05–1660	158.97–3676	–(4.08–4.96)	59.84–745.9	25.7–745.9	44.65–1807	151.3–3696	33.43–2685	158.81–4123
	$\Delta E_{\mathbf{G}}^{\mathbf{out}}$ [%]	–	*Ref*	–(5.53–13.8)	(−13.3)–105.2	683–61468	784.5–40768	598.8–55767	831.0–69643	*Ref*	–(5.39–18.5)	(−18.5)–77.5	321–54609	784.5–40768	338.1–45882	820.9–69643
	$\Delta E_{\mathbf{PV}}$ [%]	–	*Ref*	0	0	–(53.30–75.90)	0	–(60.39–74.21)	–(61.57–75.74)	*Ref*	0	0	–(62.10–77.45)	0	–(62.56–77.35)	–(61.89–75.74)
	$\Delta E_{\mathbf{HP}}$ [%]	–	–	*Ref*	0	–(4.19–21.06)	102.3–313.2	(−49.06)–101.14	102.3–313.2	–	*Ref*	0	–(2.50–21.08)	102.3–313.2	(−51.71)–151.44	102.3–313.2
	$\Delta E_{\mathbf{BESS}}^{\mathbf{in}}$ [%]	–	–	–	*Ref*	(−1.674)–102.9	(−5.52)–0	10.99–96.43	61.86–89.74	–	–	*Ref*	30.18–125.4	(−5.52)–0	(−7.08)–167.34	61.34–89.97
	$\Delta C_{\mathbf{BESS}}$ [%]	–	–	–	*Ref*	–(0.312–1.773)	0–0.240	–(0.610–1.691)	–(0.981–1.442)	–	–	*Ref*	(−2.05)–0.0814	0–0.240	–(−2.83)–0.1769	–(0.973–1.454)
	$\Delta E_{\mathbf{HP}}^{\mathbf{TESS}}$ [%]	–	–	–	–	–	*Ref*	–(21.05–97.37)	0	–	–	–	–	*Ref*	–(34.87–97.37)	0
	$\Delta Q_{\mathbf{TESS}}$ [%]	–	–	–	–	–	*Ref*	(−68.22)–8.33	0	–	–	–	–	*Ref*	(−68.22)–24.30	0
Summer	$V_{0.95}$ [%]	3.258	3.11–3.17	3.17–3.24	3.17–3.24	3.10–3.36	3.89–5.21	3.10–3.41	3.36–4.22	2.85–2.94	3.05–3.14	3.05–3.14	2.94–3.16	10.50–11.28	3.06–3.34	8.66-9.52
	$V_{1.05}$ [%]	0	0	0	0	0	0	0	0	0–0.55	0–0.44	0–0.44	0–0.235	0–0.0712	0	0
	$V_{0.90}$ [%]	0.020	0.0044	0.10–0.12	0.10–0.12	0.00692–0.050	0.295–0.392	0.00593–0.0731	0.1978–0.220	0.0044	0.21–0.23	0.21–0.23	0.00742–0.0494	1.165–1.929	0.0249–0.131	0.673-0.918
	$V_{1.10}$ [%]	0	0	0	0	0	0	0	0	0	0	0	0	0	0	0
	ΔC_E [%]	*Ref*	–(165.0–242.9)	–(49.0–180.8)	–(49.0-180.8)	–(51.25–182.8)	(−149.7)–394.6	(−267.4)–814.0	(−51.14)–636.2	–(164.8–242.9)	–(49.0–180.8)	–(49.0-180.8)	(−251.8)–18.86	(−148.9)–473.6	(−33.69)–1151	(−71.77)–762.3
	$\Delta C_{E,g}$ [%]	*Ref*	–(165.0–242.9)	–(93.21–136.5)	–(93.21–136.6)	–(88.73–111.0)	–(34.09–125.7)	(−132.5)–13.86	–(1.906–71.75)	–(164.8–242.9	–(93.21–137.2)	–(93.21–137.3)	(–58.19–118.52)	–(34.09–125.7)	(−70.94)–42.02	–(1.590–81.83)
	$\Delta E_{\mathbf{G}}^{\mathbf{in}}$ [%]	*Ref*	–(30.57–39.64)	(−31.0)–107.3	(−31.1)–107.3	3.03–943.67	32.81–1971	20.71–1988	56.14–2188	–(30.57-39.81)	(−31.0)–107.3	(−31.1)–107.3	(−17.73)–981.8	32.81–1971	(−13.43)–1861	25.78–2187
	$\Delta E_{\mathbf{G}}^{\mathbf{out}}$ [%]	–	*Ref*	–(3.32–9.03)	–(3.32–9.03)	(−40.34)–359.3	(−15.51)–277.2	(−67.85)–284.6	(−55.66)–325.9	*Ref*	–(3.30–9.52)	–(3.30–9.52)	(−44.00)–406.5	(−14.83)–291.9	(−79.95)–340.5	(−55.20)–345.9
	$\Delta E_{\mathbf{PV}}$ [%]	–	*Ref*	0	0	–(40.63–80.01)	0	–(8.95–56.62)	–(44.11–50.65)	*Ref*	0	0	–(30.24–52.98)	0	–(9.00–64.39)	–(44.14–50.69)
	$\Delta E_{\mathbf{HP}}$ [%]	–	–	*Ref*	0	(−1.631)–1	477.0–941.1	288.9–272.1	477.0–941.1	–	*Ref*	0	(−2.47)–0	477.0–941.1	131.3–737.3	477.0–941.1
	$\Delta E_{\mathbf{BESS}}^{\mathbf{in}}$ [%]	–	–	–	*Ref*	37.47–62.12	(−1.631)–0	42.73–102.9	32.08–55.89	–	–	*Ref*	37.98–63.52	(−1.631)–0	29.69–97.04	31.76–51.23
	$\Delta C_{\mathbf{BESS}}$ [%]	–	–	–	*Ref*	–(0.545–1.020)	0–0.0611	–(0.661–1.770)	–(0.461–0.900)	–	–	*Ref*	–(0.558–1.008)	0–0.0611	–(0.431–1.621)	–(0.453–0.789)
	$\Delta E_{\mathbf{HP}}^{\mathbf{TESS}}$ [%]	–	–	–	–	–	*Ref*	–(5.21–48.60)	0	–	–	–	–	*Ref*	–(13.95–59.56)	0
	$\Delta Q_{\mathbf{TESS}}$ [%]	–	–	–	–	–	*Ref*	(−1.612)–6.45	0	–	–	–	–	*Ref*	0–6.45	0

Table 4
Result ranges per season for different adoption levels (60%–80%).

		0%	60%							80%						
			1	2	3	4	5	6	7	1	2	3	4	5	6	7
Winter	$V_{0.95}$ [%]	3.263	3.26	12.84–13.53	12.81–13.50	3.94–4.74	27.26–28.18	3.47–3.85	26.58–27.37	3.26	14.44–14.47	14.38–14.41	5.05–5.62	27.26–28.33	4.18–4.30	26.87–27.15
	$V_{1.05}$ [%]	0	0	0	0	0–0.0465	0–0.0934	0–0.0618	0–0.207	0	0	0	0.229–0.426	0.890–1.212	0.309–0.586	1.580–2.34
	$V_{0.90}$ [%]	0.020	0.020	1.14–1.83	1.13–1.86	0.1622–0.1834	14.89–15.73	0.0524–0.0999	11.62–12.57	0.020	4.45–4.88	4.44–4.88	0.269–0.302	22.32–22.72	0.1305–0.1869	21.52–22.01
	$V_{1.10}$ [%]	0	0	0	0	0	0	0	0	0	0	0	0	0	0	0
	ΔC_E [%]	*Ref*	–(5.40–6.84)	10.76–323	5.18–322	55.57–835.2	21.22–954.9	29.35–614	33.27–1183	–(5.35–6.84)	10.76–307.76	5.18–308	39.26–805.4	21.22–910.2	30.02–788.9	45.23–1169
	$\Delta C_{E,g}$ [%]	*Ref*	–(5.40–6.84)	–(52.68–78.85)	–(55.06–78.56)	–(40.01–74.64)	–(44.64–65.67)	–(55.28–73.84)	–(32.43–62.51)	–(5.35–6.84)	–(52.68–78.66)	–(55.06–78.66)	–(40.81–77.98)	–(44.60–65.96)	–(44.52–73.10)	–(33.03–62.37)
	$\Delta E_{\mathbf{G}}^{\mathbf{in}}$ [%]	*Ref*	–(3.92–4.87)	41.52–745.9	35.52–746	70.61–1591	99.71–3696	33.99–1460	107.6–4102	–(3.92–4.96)	41.52–737.1	35.52–737	43.85–1686	99.71–3653	34.09–1978	107.6–4079
	$\Delta E_{\mathbf{G}}^{\mathbf{out}}$ [%]	–	*Ref*	–(5.40–18.50)	(−18.5)–77.51	297.0–31107	458.96–40768	(−39.26)–34987	326.3–69643	*Ref*	–(4.98–19.96)	(−20.0)–105.2	(−34.95)–53026	458.96–40768	(−38.37)–43960	326.3-5-3454
	$\Delta E_{\mathbf{PV}}$ [%]	–	*Ref*	0	0	–(61.86–77.58)	0	–(60.42–81.35)	–(61.89–75.74)	*Ref*	0	0	–(53.22–77.72)	0	–(54.16–77.47)	–(59.9–75.74)
	$\Delta E_{\mathbf{HP}}$ [%]	–	–	*Ref*	0	–(2.36–21.08)	102.28–313.22	(−52.06)–99.39	102.3–313.2	–	*Ref*	0	–(2.32-24.07)	102.28–313.22	(−54.42)–59.96	102.3–313.2
	$\Delta E_{\mathbf{BESS}}^{\mathbf{in}}$ [%]	–	–	–	*Ref*	(−4.05)–149.1	(−5.52)–0	(−7.45)–173.2	61.76–90.50	–	–	*Ref*	(−20.12)–145.7	(−9.58)–0	(−10.37)–164.0	61.76–89.98
	$\Delta C_{\mathbf{BESS}}$ [%]	–	–	–	*Ref*	(−2.42)–0.1226	0–0.240	(−2.98)–0.1828	–(0.983–1.453)	–	–	*Ref*	(−2.40)–0.419	0–0.264	(−2.83)–0.233	–(0.989–1.454)
	$\Delta E_{\mathbf{HP}}^{\mathbf{TESS}}$ [%]	–	–	–	–	–	*Ref*	–(48.72–97.90)	0	–	–	–	–	*Ref*	–(61.23–97.90)	0
	$\Delta Q_{\mathbf{TESS}}$ [%]	–	–	–	–	–	*Ref*	(−69.07)–34.58	0	–	–	–	–	*Ref*	(−69.07)–31.78	0
Summer	$V_{0.95}$ [%]	3.258	2.83–2.84	3.37–3.53	3.33–3.53	2.73–2.92	13.39–13.74	3.60–3.89	12.62–12.74	2.82–2.83	4.04–4.12	4.04–4.12	2.68–2.95	15.22–15.57	4.29–4.42	14.22–14.39
	$V_{1.05}$ [%]	0	2.40–3.18	2.03–2.69	2.03–2.69	1.170–2.39	0.466–1.406	0.0168–0.555	0.0420–1.191	5.40–6.16	4.79–5.54	4.79–5.54	5.03–5.75	3.971–4.556	1.412–1.645	3.10–3.47
	$V_{0.90}$ [%]	0.020	0.0044	0.31–0.33	0.31–0.33	0.0178–0.0534	5.33–5.88	0.0623–0.1315	3.31–3.80	0.0044	0.42–0.47	0.42–0.47	0.0588–0.0751	8.80–9.06	0.1696–0.265	6.80–7.17
	$V_{1.10}$ [%]	0	0	0	0	0	0	0	0	0.023–0.314	0.01–0.26	0.01–0.26	0–0.0895	0–0.0351	0	0
	ΔC_E [%]	*Ref*	–(158.6–257.5)	–(49.02–204.3)	–(49.02–204.3)	–(719.0)–158.7	(−176.7)–473.6	(−219.6)–949.5	(−39.88)–706.6	–(158.6–257.5)	–(49.02–204.3)	–(49.02–204.3)	(−723.7)–180.7	(−176.7)–473.6	(−342.0)–514.9	(−72.30)–766.4
	$\Delta C_{E,g}$ [%]	*Ref*	–(158.6–257.5)	–(93.21–158.5)	–(93.21–160.5)	–(38.89–180.8)	–(34.09–149.4)	(−115.6)–8.92	–(1.906–71.75)	–(158.6–257.5)	–(93.21–158.5)	–(93.21–160.5)	–(37.23–181.6)	–(34.09–149.4)	–(154.6–0.475)	–(1.619–82.17)
	$\Delta E_{\mathbf{G}}^{\mathbf{in}}$ [%]	*Ref*	–(30.6–39.8)	(−34.8)–107.3	(−36.63)–107.3	(−20.04)–973.87	6.83–2049	(−12.77)–1543	61.66–2277	–(30.6–39.6)	(−34.8)–107.3	(−36.63)–107.3	3.14–1011	6.83–1971	9.40–1809	25.71–2188
	$\Delta E_{\mathbf{G}}^{\mathbf{out}}$ [%]	–	*Ref*	–(3.00–9.52)	–(3.00–9.52)	(−51.20)–446.2	(−15.80)–291.9	(−89.01)–323.1	(−56.82)–344.4	*Ref*	–(3.00–9.57)	–(3.00–9.57)	(−47.30)–462.0	(−15.51)–289.8	(−86.1)–373.4	(−56.51)–344.4
	$\Delta E_{\mathbf{PV}}$ [%]	–	*Ref*	0	0	–(28.23–55.12)	0	–(8.31–82.67)	–(43.64–50.69)	*Ref*	0	0	–(26.06–57.84)	0	–(8.31–79.61)	–(44.24–50.69)
	$\Delta E_{\mathbf{HP}}$ [%]	–	–	*Ref*	0	(−5.43)–0	477.0–941.1	128.0–716.7	477.0–941.1	–	*Ref*	0	(−5.64)–0.1621	477.0–941.1	151.89–638.0	477.0–941.1
	$\Delta E_{\mathbf{BESS}}^{\mathbf{in}}$ [%]	–	–	–	*Ref*	35.57–67.53	(−1.631)–0	24.43–111.3	32.09–53.49	–	–	*Ref*	35.12–67.00	(−1.631)–0	35.95–115.2	31.80–52.73
	$\Delta C_{\mathbf{BESS}}$ [%]	–	–	–	*Ref*	–(0.511–1.095)	0–0.611	–(0.363–1.882)	–(0.456–0.831)	–	–	*Ref*	–(0.500–1.082)	0–0.611	–(0.545–1.941)	–(0.455–0.843)
	$\Delta E_{\mathbf{HP}}^{\mathbf{TESS}}$ [%]	–	–	–	–	–	*Ref*	–(15.38–70.94)	0	–	–	–	–	*Ref*	–(20.47–69.36)	0
	$\Delta Q_{\mathbf{TESS}}$ [%]	–	–	–	–	–	*Ref*	0–6.45	0	–	–	–	–	*Ref*	(−1.613)–9.68	0

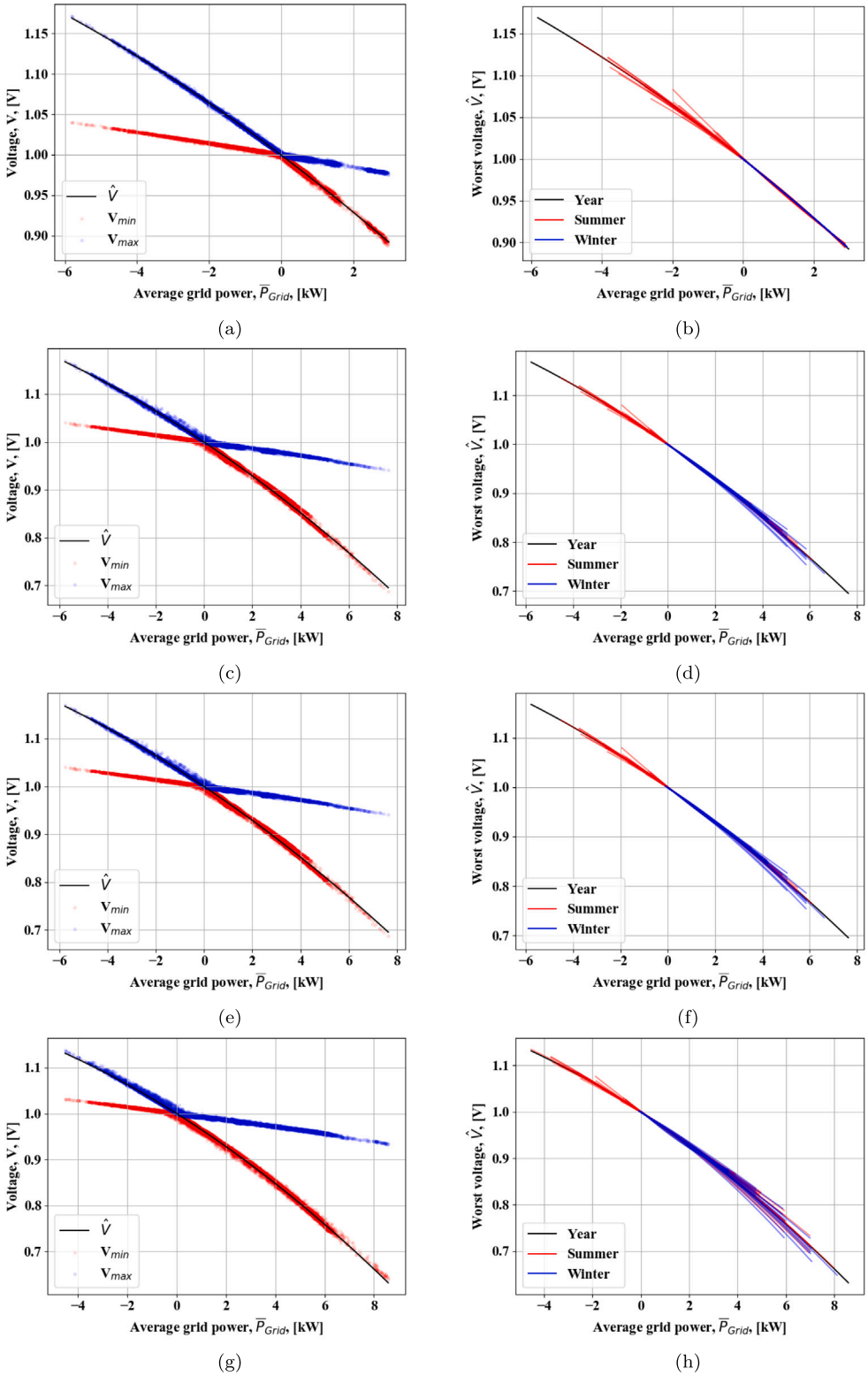

Fig. 5. Relationship between the average power and the minimum and maximum voltage in the network (a, c, e, g), and results for all scenarios and adoption levels during winter, summer and yearly (100% adoption) (b, d, f, h) for scenarios 1, 2, 3 and 5 respectively. (For interpretation of the references to colour in this figure legend, the reader is referred to the web version of this article.)

distinction between house types is less abrupt for the change in energy cost and has the same pattern as the change in electricity cost, as can be observed in Figs. 9(d) and 9(f).

Adding a battery did not make a significant change in almost any metric, as shown in Tables 3 and 4. Comparing scenarios 2 and 3 shows a small decrease in the purchase of energy from the grid and a relatively higher increase in energy export during winter. This is explained by the nominal difference between the import and export of energy during winter. Due to the low irradiance during winter, the export to the grid is very low, so a small increase in the consumption from the BESS

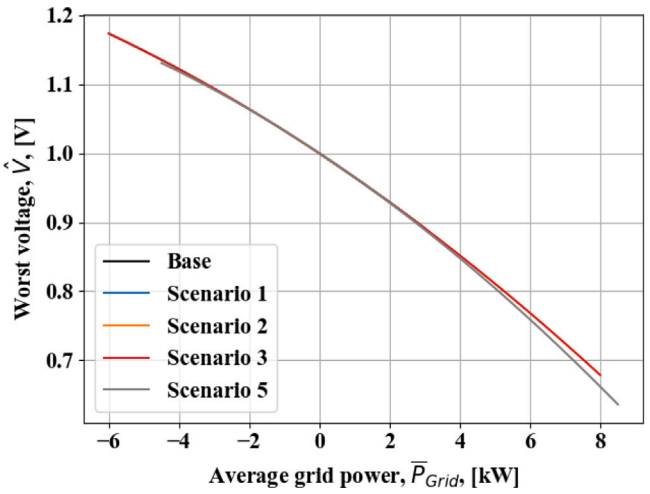

Fig. 6. Comparison of the yearly correlations between the worst voltage on the network and the average grid power for scenarios 0, 1, 2, 3 and 5.

during the low-price timeframes, to then inject it into the grid during the high-price timeframes creates a significant relative change in the energy exports of several orders of magnitude, particularly in scenario 5 (see Fig. 10(e)). This phenomenon is not as predominant in summer, as the generation exceeds the consumption during most cases, so the role of the BESS is neglectable for scenarios 2 and 3 (see Figs. 10(a) and 10(c)). For scenario 5, the more frequent activity of the BESS resulted in higher energy injections, as shown in Fig. 10(f).

Unlike the other components, the effects of the TESS are more notorious throughout the metrics shown in Tables 3 and 4. The increased energy consumption by the heat pumps to charge the TESS is reflected in the spike of both the change in energy consumption (see Figs. 8(e) and 8(f)) and voltages below 0.95 p.u. from scenarios 1–3 to 5, causing non-compliances even in adoptions below 20%. Nevertheless, the flexibility in the sources of thermal energy resulted in an increased energy export directly from the PV during the high-price timeframes, reducing the usage of the BESS (lower $E^{\text{in}}_{\text{BESS}}$ and therefore its degradation ΔC_{BESS}) in scenario 5. The effect of adding a thermal storage system on energy costs is also not an improvement when compared with scenarios 2 and 3. Despite outperforming scenario 1 during winter, scenario 5 is the least economically attractive during summer (see Fig. 9).

The role of the aggregator had significant changes in the metrics. From the network perspective, when the prosumers follow the setpoint provided by the aggregator always (scenarios 4 and 6), the voltage in the network remains within the ±0.05 p.u. during 95% of the time for adoptions up to 80% in scenario 6, and 60% in scenario 4, and very rarely below 0.9 p.u. (maximum 0.302% of the time in scenario 4 and maximum 0.1869% of the time in scenario 6). This is accomplished by drastic changes in the internal power dispatch from the EMS. Comparing scenarios 3 and 4 shows a noticeable decrease in the usage of the heat pump. Similarly, the amount of energy consumed decreased considerably when comparing scenarios 6 and 5. To minimize the injection of energy, the BESS was used more often – thus degraded –, mostly from energy purchased from the grid as the PV curtailment increased, and less energy was used to charge the TESS $E^{\text{TESS}}_{\text{HP}}$, reducing its availability for thermal power dispatch Q_{TESS}.

For most of the households, this reduction in consumption was translated into a reduction of costs, particularly in winter, by the mere fact that less energy was purchased. Nonetheless, this reduction also led to lower indoor temperatures, as shown in Fig. 11, particularly during winter. When the setpoint was not enforced in scenario 7 (semi-aggregated), small differences are noticed with scenario 5 (no aggregation), most notably on the usage of the BESS, charged from the grid, and the curtailment of PV generation. Interestingly, Fig. 11 also shows that scenarios 2 and 3 tend to have lower temperatures than the others without an aggregator. This is due to the operation strategy for the heat pump; it is not used in high-price timeframes that might coincide with higher setpoint temperatures, and in low-price timeframes (during the night), the setpoint is lower. This way, the TESS provides flexibility to the heat generation so that the indoor temperature remains higher without considerably changing the energy cost.

Provided that there is a benefit in the MCES for both the prosumer and the DSO, we estimated the minimum compensation each prosumer would require to make it profitable to support the DSO (scenario 6). We used scenario 2 (PV+HP) as a reference since previous work recommended such a combination for Dutch houses to eliminate the dependency on gas [29]. To define the capital expenses of the MCES per house, we used 1.15 €/W for the PV (sized per house) with a minimum value of €2500, €6500 for the heat pump, €10 000 for the BESS and €25 000 for the underground TESS and run scenarios 2 and 6 for one year considering a 100% adoption to estimate their revenue for each household on the worse case for the grid. The revenue considers the profit earned by the normal operation of the system under the existing market conditions for each scenario compared to the base scenario.

For the support scenarios to be attractive to prosumers, they should be, at least, as profitable as the case without supporting the grid. In this case, scenario 2 was selected as the reference, based on a fully-electrified heating condition. Fig. 12 shows the minimum requirements for scenarios 4 and 6 to have the same ROI as scenario 2. Scenarios 4 and 6 had similar changes in energy cost (see Tables 3 and 4), however, the capital expenses for scenario 4 are considerably lower due to the high cost of the TESS. Fig. 12(a) shows that the average energy cost is higher than the monthly compensation required for scenario 4 to have the same ROI as scenario 2, and Fig. 12(b) shows, per household, the difference between the cost and the required compensation. Fig. 12(c) compares the compensation required per household for scenario 6, so that the ROI is the same as scenario 2. The results indicate that the compensation and costs behave fairly similar, and the compensation is mostly greater until consumption is around 7 MWh/year, where the energy cost is higher than the compensation required. Then, Fig. 12(d) shows the difference per household.

4.3. Centralized storage

Following (34), we estimated the accumulated voltage incompliance per node for each case, grouped per adoption level, during winter and summer. Fig. 13 shows the results. For scenario 1, the adoption does not greatly affect the incompliance during winter because there is little generation, and the incompliances are due to the base congestion in the grid (see Fig. 13(a)). During summer, however, increasing the adoption does increase the incompliance due to energy injection, as indicated in Table 4 (see Fig. 13(b)). The summer in compliance for scenario 2 is fairly similar to scenario 1, as the higher temperatures require lower usage of the heat pumps (see Fig. 13(d)), but during winter, the incompliances increase considerably, and proportionally to the adoption, due to the energy used by the heat pumps, as mentioned in Tables 3 and 4 (see Fig. 13(c)). For three of the four cases (winter and summer in scenario 1, and summer in scenario 2), the most critical node was 270. For winter in scenario 2, the most critical node was 238, but node 270 still remained critical. For this reason, we chose node 270 to place the centralized system.

Initially, a 1 MWh/1 MW BESS system coupled with a 200 kW PV system is considered. However, it was insufficient for adoptions above 60%. Thus, the capacity of the BESS was increased to 2 MWh for the 60% adoption and to 10 MWh for the 80% adoption. No improvements were observed above those values. Similarly, increasing the PV system did not show any major benefit as, during winter, the generation is almost neglectable in comparison with the demanded

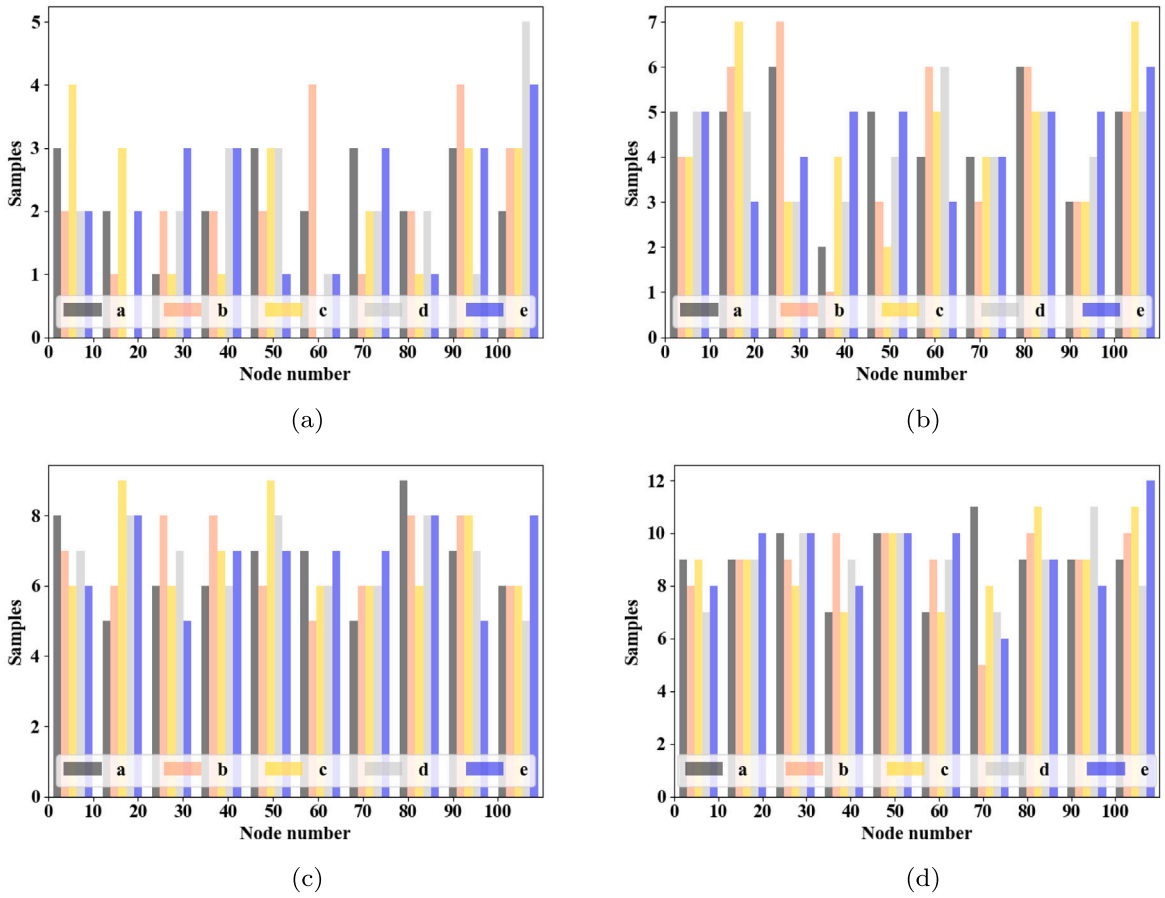

Fig. 7. Distribution of nodes selected per case, per adoption percentage (20%, 40%, 60% and 80%, respectively).

Table 5
BESS and PV system sizes per adoption level of PV+HP for case 8.

Adoption	BESS	PV
20%	1 MWh, 1 MW	200 kW
40%	1 MWh, 1 MW	200 kW
60%	2 MWh, 1 MW	200 kW
80%	10 MWh, 1 MW	200 kW

power, and during summer, most of the generation above that threshold was curtailed to avoid overvoltages. Table 5 lists the sizes considered per adoption level for the assets, and Table 6 summarizes the voltage results per adoption level per season. During summer, the network does not require external assistance to comply with the voltage limits (see Table 4). Still, the BESS is capable of improving the network behaviour for adoptions up to 60%. At 80%, the BESS can compensate for the overvoltages by consuming power from the grid, at the cost of increasing the undervoltages. In winter, however, the central system cannot ensure compliance with the standard EN50160. Despite the worse node being compensated, other nodes remained with little or no change before and after including the centralized storage, as shown in Fig. 14, and the BESS have to consume almost all the energy used to compensate the grid from the grid itself, as the PV generation is almost neglectable in comparison with the energy required to compensate for the grid.

5. Discussion

After presenting the results in Section 4, some correlations became notorious, leading to consequences both for the prosumer and the DSO. In both cases, changing the system architecture would result in different power dispatches. Removing the gas boiler naturally would transfer all the thermal load to the electrical network through the heat pumps, however, adding storage devices might shift or shave the consumption peaks. In this work, we used the same EMS strategy for every house. Even though each house has different electric and thermal load conditions, the day-ahead prices for all will be the same. Particularly for scenarios 2–5 and 7, which are very heavily dependent on prices to minimize the cost for the prosumer, an unconscious synchronization of peaks is to be expected. The effect is consistent with the results in [6], where the local EMSs react to the changes in energy price simultaneously, consuming or injecting energy accordingly. As a result, the prosumers would use controllable high-power appliances, such as the BESS or the HP, during low-price periods, creating congestion. This phenomenon will increase with the adoption, as shown in Tables 3 and 4, where the voltages for scenarios 2, 3, 5 and 7 consistently drop in the absence of an aggregated control.

Under the existing residential energy market and energy storage costs, investing in energy storage is not attractive. Nevertheless, the previous analysis suggests that there is an opportunity for a energy market mechanism based on supporting the network using BESS at the residential level. This is because the total energy cost is still above the compensation (see Fig. 12(a)), thus, both the DSO and the prosumer have room for profit. However, TESS high costs make it more challenging. The required compensation goes above the energy costs, meaning that the prosumer must be paid to consume energy, as shown in Fig. 12(b). For both cases, external funding could accelerate the market towards decreasing energy storage costs. For instance, subsidies for purchase or operation could reduce costs, making the business case more attractive for prosumers and the DSO.

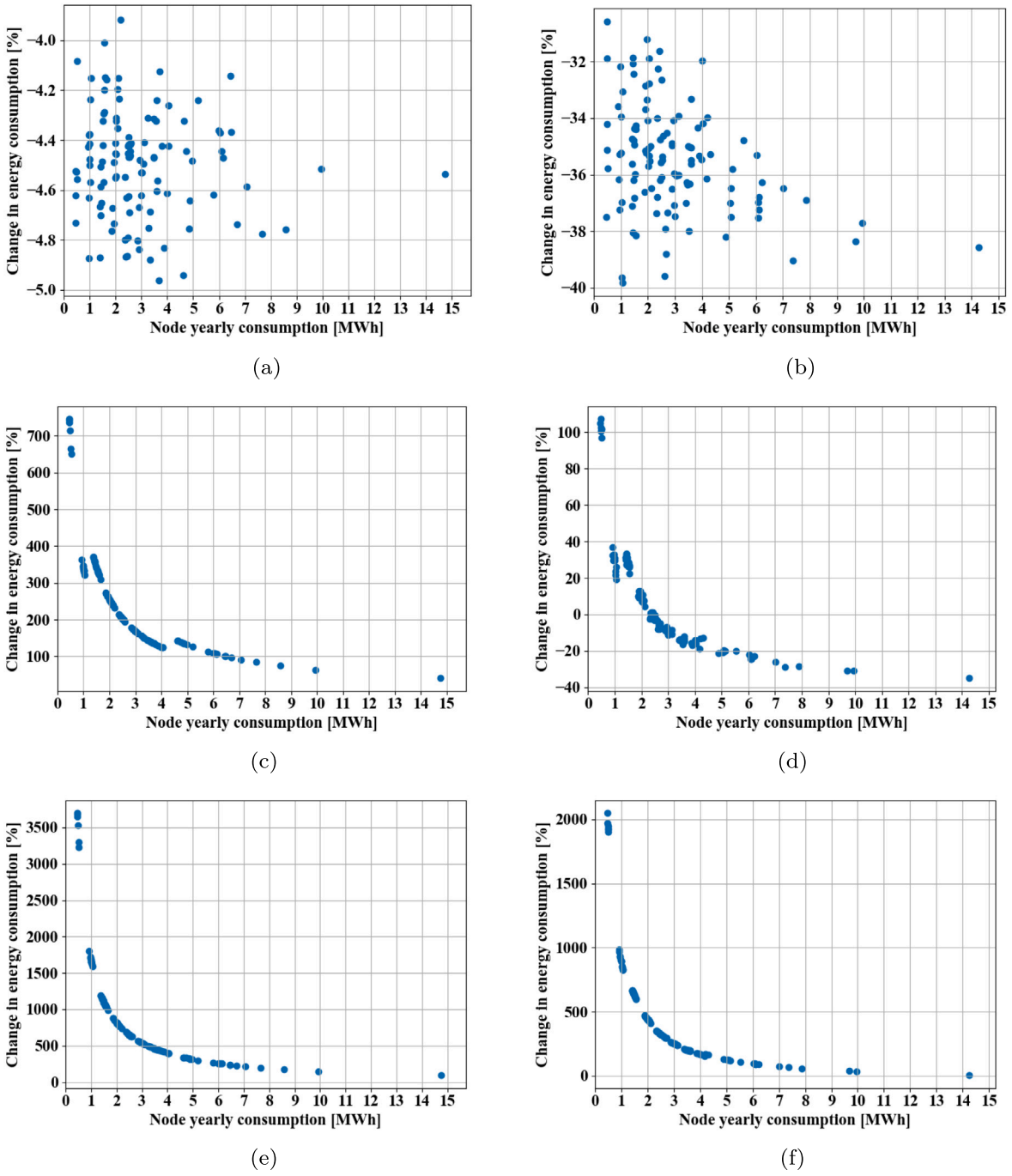

Fig. 8. Distribution of the change in energy consumed from the grid per household for scenarios 1,2 and 5 during a week in winter (a), (c), (e) and summer (b), (d), (f), respectively.

Table 6
Result ranges per season for different adoption levels of PV+HP for case 8.

Adoption [%]	Winter				Summer			
	$V_{0.95}$ [%]	$V_{1.05}$ [%]	$V_{0.90}$ [%]	$V_{1.1}$ [%]	$V_{0.95}$ [%]	$V_{1.05}$ [%]	$V_{0.90}$ [%]	$V_{1.1}$ [%]
20	0.1898–1.150	0	0–0.0717	0	0.200–0.236	0	0	0
40	4.18–5.28	0	0.240–0.267	0	0.259–0.402	0.00005–0.438	0	0
60	8.87–9.25	0.0005	0.621–1.156	0	0.475–0.617	1.981–2.59	0–0.0252	0
80	10.96–11.18	0.007–0.01	1.902–2.08	0	6.87–6.92	4.71–5.45	0.293–0.311	0.0089–0.257

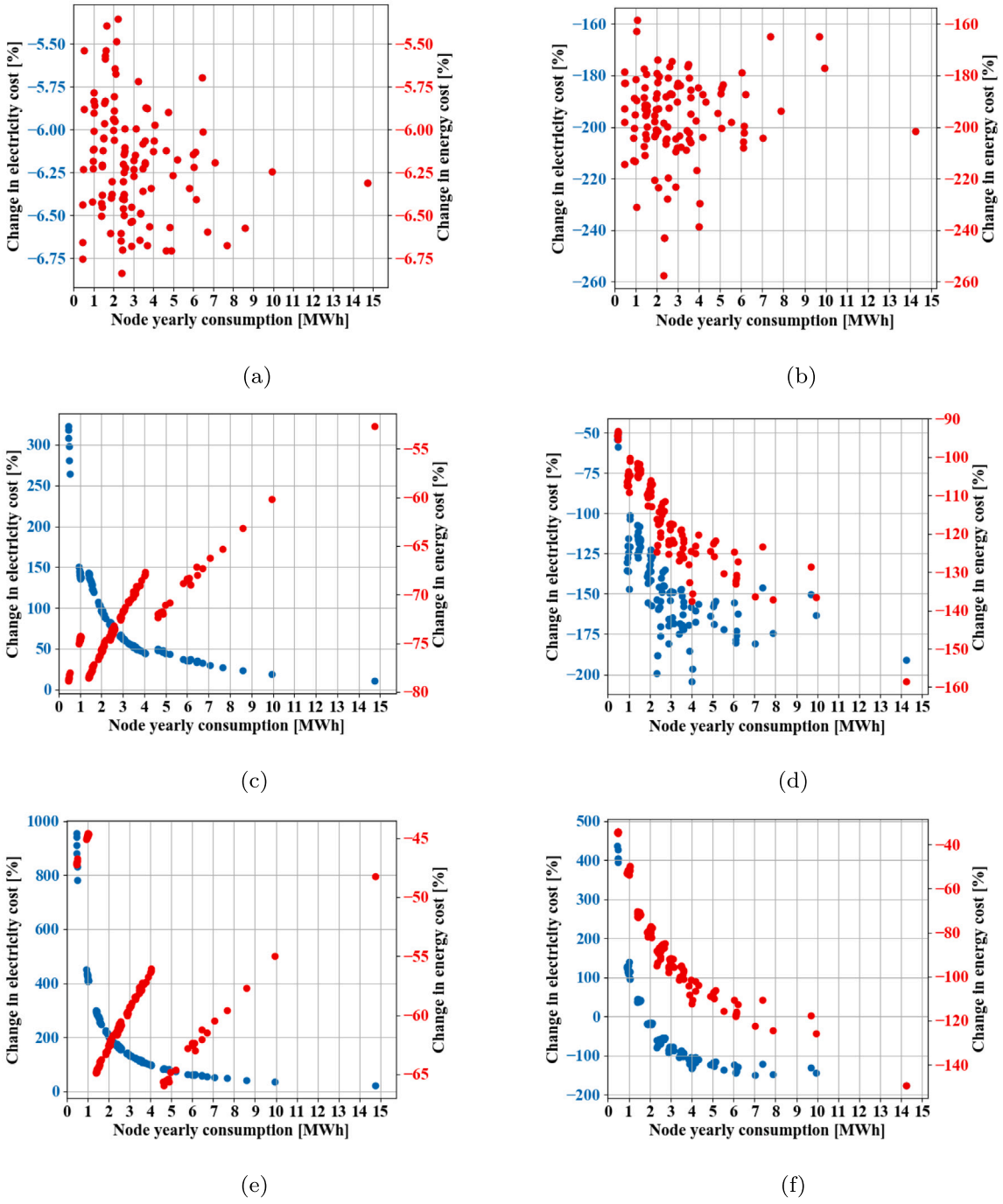

Fig. 9. Distribution of the change in energy cost from the grid per household for scenarios 1,2 and 5 during a week in winter (a), (c), (e) and summer (b), (d), (f), respectively.

The same logic can be applied in reverse order if an aggregator has observability over the network's voltages and powers. In that case, the aggregator can define a power setpoint to minimize those violations. As shown in scenario 6, when the setpoint defined by the aggregator is enforced, there is a clear drop in undervoltages, consistent with [33]. Nevertheless, the prosumers require flexible loads and energy sources to be able to meet the setpoint. In this sense, both the BESS and the TESS play a key role. On the one hand, the BESS can store or dispatch electric power, either to supply the local demand or to directly support the grid. Similarly, the thermal storage could provide thermal power in a restrictive event when the heat pump would contribute to high congestion. Both effects are shown in our simulations, but cannot be generalized. Instead, our results suggest that this would depend on the load conditions. From an electrical point of view, in some cases, the load would match with the PV generation, and the electrical storage is less critical, leading to different patterns of energy supplied by the BESS, as shown in Tables 3 and 4. For the thermal storage, smaller spaces, characterized by lower electric and thermal demand, benefit from the thermal storage, as the thermal demand can be met with the TESS, whereas bigger houses have larger thermal demands and would require a larger TESS to reduce their dependency on the heat pump.

From a cost perspective, the more devices comprise the system, the higher the revenue is required to justify the system acquisition. The change in cost presented in Section 4 demonstrated that, in fact, more complex systems do not guarantee lower relative costs compared to the base scenario. During summer, only a PV system (scenario 1)

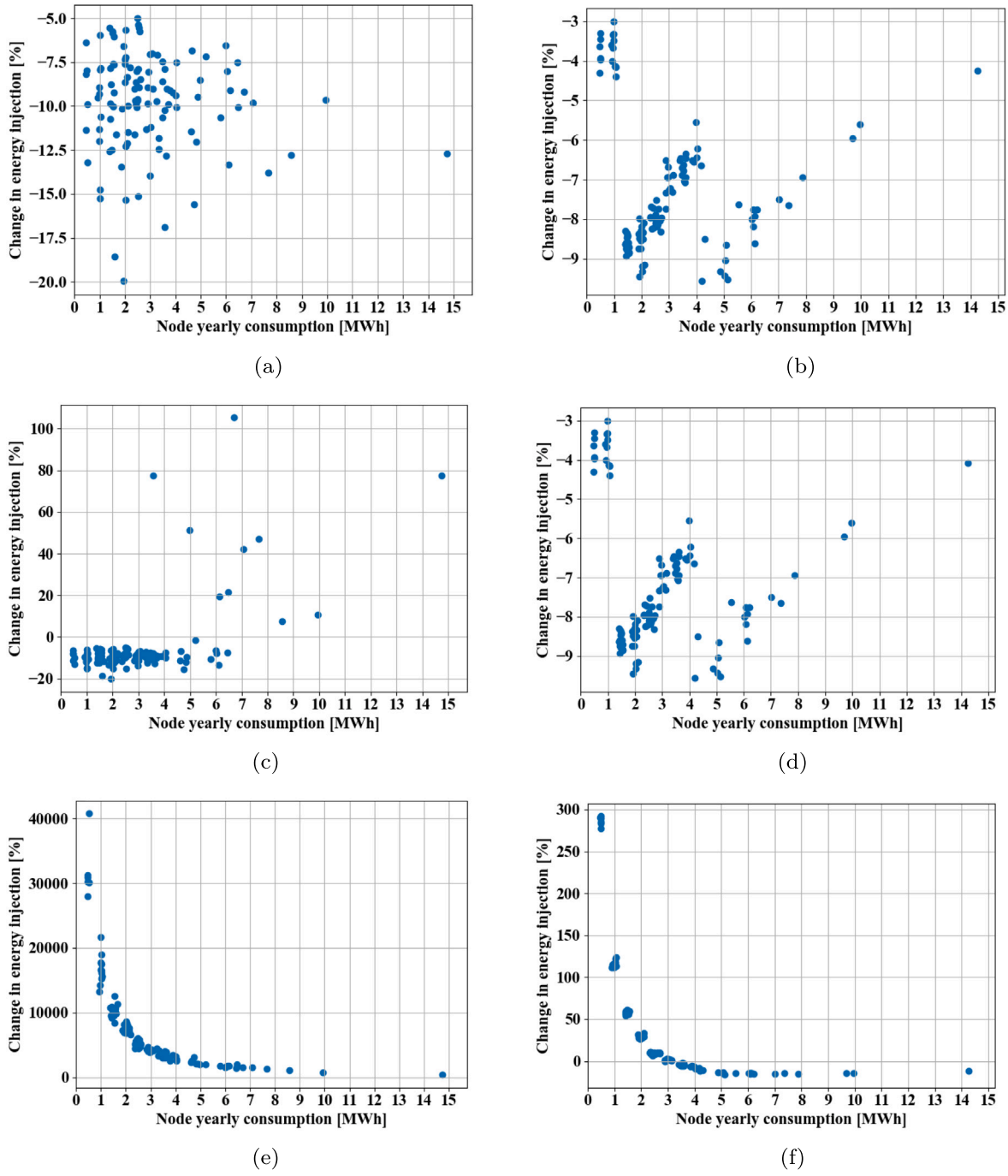

Fig. 10. Distribution of the change in energy injected to the grid per household for scenarios 2, 3 and 5 during a week in winter (a), (c), (e) and summer (b), (d), (f), respectively.

results in the most profitable since the higher temperatures require lower usage of the thermal elements (i.e., heat pump and TESS). During winter, combining the PV with a heat pump is the most profitable architecture, as it eliminates the dependence on gas for heating. Adding storage elements like BESS or TESS did not demonstrate any economic benefit for either of the three aggregation scenarios given the current market mechanism (day-ahead pricing considering feed-in tariff and no compensation for supporting the grid) and would require higher investments, making them unattractive for prosumers, despite their benefits for the DSO. However, previous works suggest that new markets could make such investments attractive [34,35]. In this sense, Fig. 12 shows that given compensation, the ROI of scenarios 4 and 6 can be reduced to the ROI of scenario 2. Scenario 4 might be an interesting business case, as the compensation prosumers require is below the overall energy cost (see Fig. 12(a)). However, scenario 6 might not be attractive to DSOs, as the compensation would go beyond the energy costs for low- to mid-consumption prosumers (see Fig. 12(c)). Instead, additional schemes can be considered. For example, providing not a total but a partial compensation to the prosumer below the energy cost or involving governmental institutions to provide subsidies in this kind of investment under the condition of collaboration with the DSO.

DSOs are required to ensure voltage conditions on the grid, as stated in the standard EN50160. Each scenario requires different levels of involvement from the DSOs to ensure the voltage conditions, based on the adoption percentage, as shown in Table 7. On the one hand, it is not expected that the adoption increases linearly with time, but

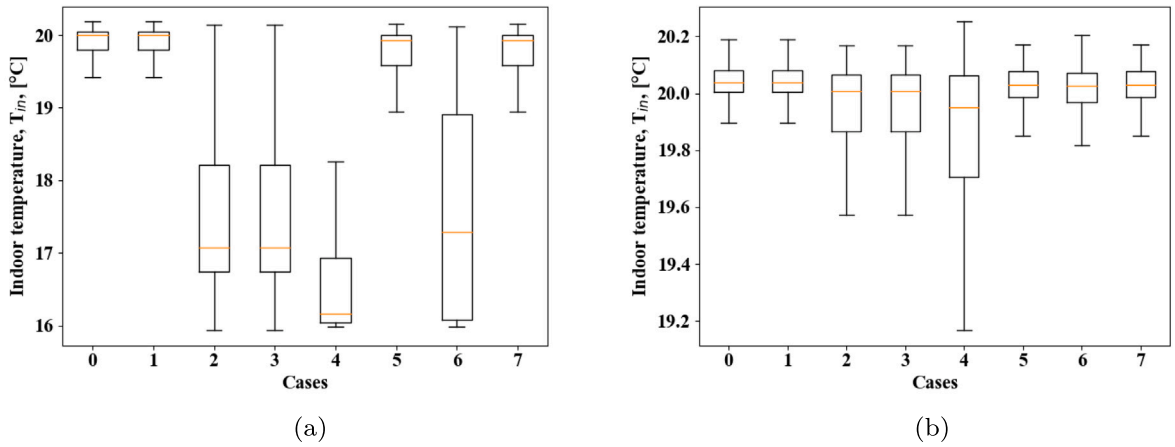

Fig. 11. Indoor temperature distribution in the houses during (a) winter, and (b) summer for each scenario.

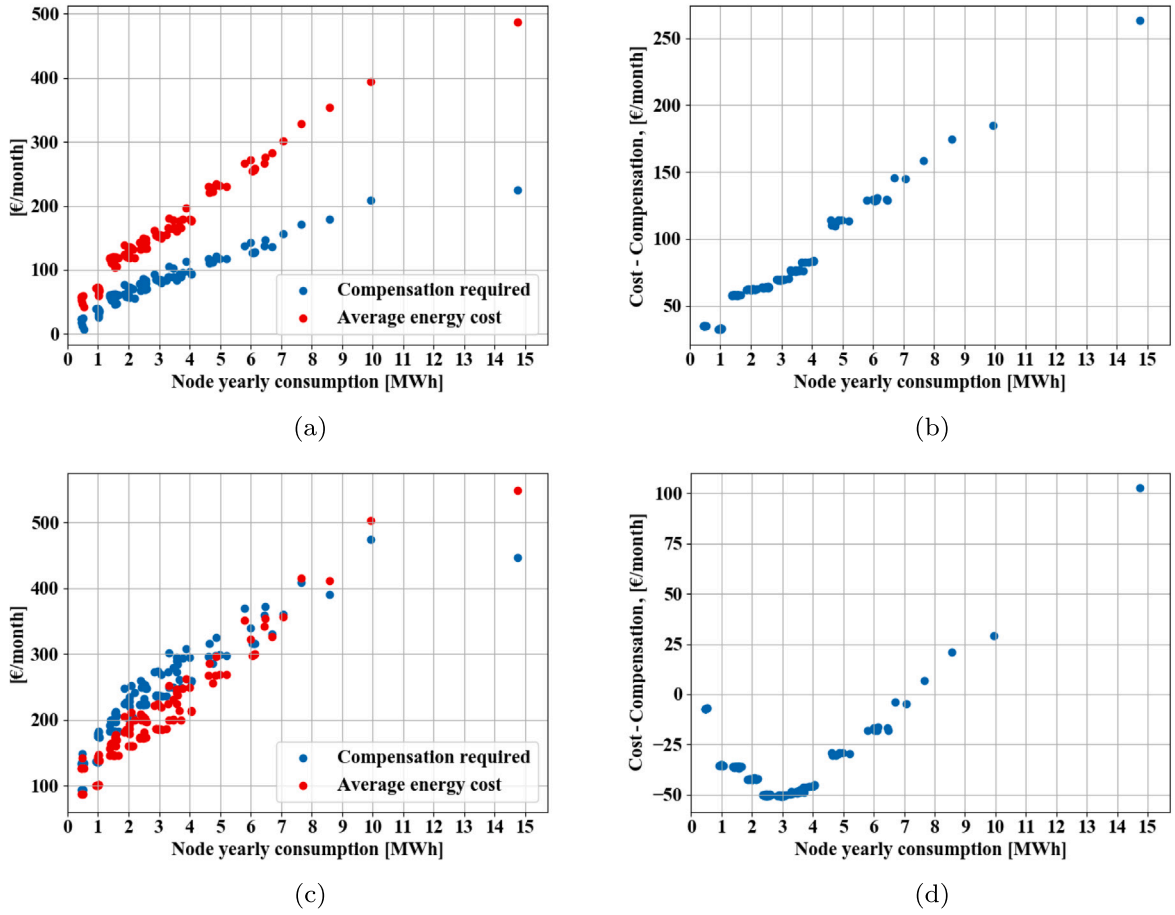

Fig. 12. Investment comparison of scenario 2 with scenarios 4 and 6, considering (a), (c) the required monthly compensation to ensure the ROIs for both scenarios are the same and (b), (d) the difference between the required compensation and the average monthly energy cost, respectively.

instead saturates at some point, from where the increase in the adoption is slower. That being said, knowing that the approach allows a later deployment of reinforcement reduces the time pressure to commission the project; the higher the adoption, the more time the DSO would have to come up with the best approach, including execution time. On the other hand, the fact that the grid can withhold larger adoptions, without changes, would also imply that the reinforcement required is smaller (to ensure minimum compliance), gaining more value from the same system, either before or after reinforcement. As can be seen, the aggregated scenarios (4 and 6) result in more reliable systems, whereas the cases without aggregation require reinforcements on the grid more urgently.

Using a centralized PV+BESS system (scenario 8) could not outperform single- nor multi-carrier aggregated storage. The results of the centralized system to compensate for the inclusion of PV and heat pumps in households shown in Table 6 demonstrate a single unit can support the network in low adoptions. However, adoptions above 60% during winter and 80% during summer show incompliance with the

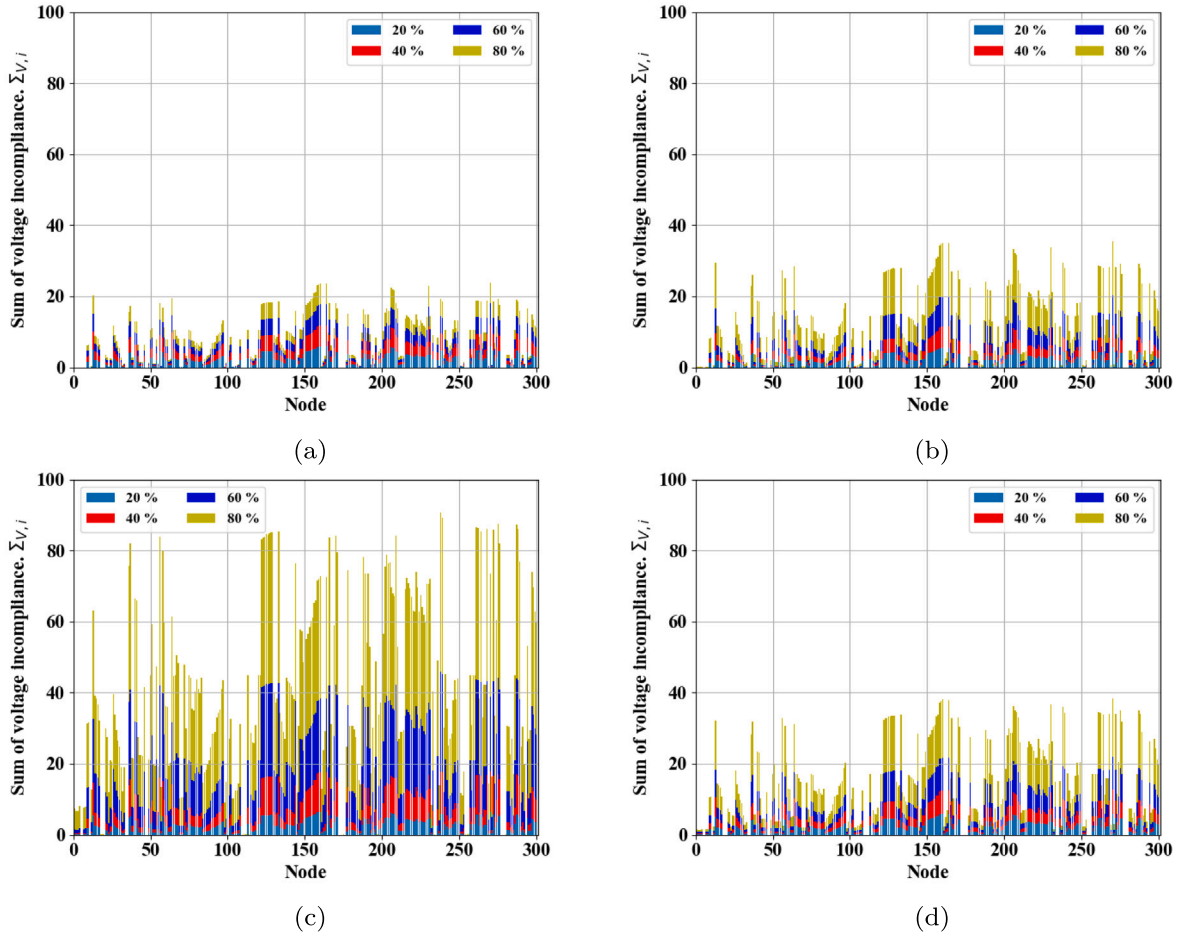

Fig. 13. Accumulated voltage incompliance per node for scenarios 1 and 2 during (a), (c) winter and (b), (d) summer, respectively.

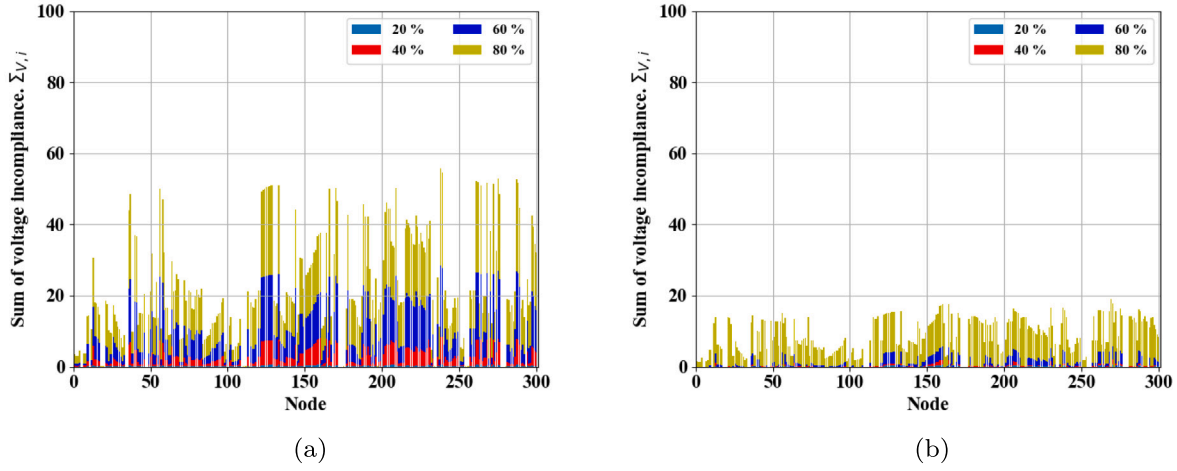

Fig. 14. Accumulated voltage incompliance per node for scenarios 8 during (a) winter and (b) summer.

standard EN50160. The reason is the distribution of power throughout the radial grid. If there are loads in branches whose nodes are far from both the substation and the centralized system, their voltage drops will not be compensated effectively, as they would in a distributed case, such as scenarios 4 and 6. In addition, the storage capacity required for a centralized system largely exceeds the sum of the household storage units. For instance, for a adoption of 40%, a system of 1 MWh is required for the centralized system, compared to 28 systems of 10 kWh used in scenarios 4 and 6 (280 kWh in total). Yet, the grid shows better behaviour with the aggregated storage during winter, as shown

Table 7
Maximum adoption ranges per scenario without violating voltage limits.

Scenario	Winter [%]	Summer [%]
1: RES inclusion	>80	>80
2: Heat electrification	20–40	>80
3: Single-carrier non-aggregated storage	20–40	>80
4: Single-carrier aggregated storage	60–80	>80%
5: Multi-carrier non-aggregated storage	0–20	0–20
6: Multi-carrier aggregated storage	>80	>80
7: Multi-carrier semi-aggregated storage	0–20	20–40
8: Centralized Storage[1]	20–40	60–80

in Table 3, where the voltage is below 0.95 p.u. during up to 3.57% of the time with the aggregated single-carrier storage and 3.46% with the aggregated multi-carrier storage, compared to the 5.28% with the central system. For higher adoptions, the central system cannot satisfy the standard EN50160, regardless of the capacity of the battery, as some nodes saw almost no change before (see Fig. 13) and after (see Fig. 14) including the central BESS.

Also, it is worth mentioning the physical capacity of the distribution system. Normally, the cabling towards the end of the distribution systems is thinner than close to the substation. This is due to the traditional, uni-directional, power flow considered for the design of those systems in the past. Thus, placing a centralized system in nodes far from the substation might require reinforcement regardless, as the cables cannot transport the current needed to compensate the voltage drop, making the centralized solution unsuitable.

6. Conclusions

This paper provided an in-depth analysis of the effects of including four architectures of residential single- and multi-carrier energy systems in a real low-voltage distribution network in the Netherlands. From the prosumer perspective, adding BESS or TESS resulted in energy cost savings between 45–66% and 34–149% in winter and summer, respectively, compared with a base case without any addition. Nevertheless, a PV+HP system results in savings between 55–79% and 93–161% during winter and summer, respectively. When considering the prosumer yearly consumption, lower consumption prosumers have worse ROIs and require compensations beyond their actual energy cost to make a profit from a multi-carrier energy storage system.

From the DSO perspective, including PV systems sized for near-net-zero buildings did not violate the minimum voltage regulations of the standard EN50160 for adoptions below 80%. Nevertheless, including heat pumps causes the voltage to be below 0.95 p.u. up to 8% of the week in winter for adoptions above 40%. Single-carrier aggregation (only batteries) provided satisfactory voltage behaviours (voltage below 0.95 p.u. during 5.62% of the time in winter) at the cost of lower indoor temperatures and higher curtailments on the prosumer side. Multi-carrier aggregation provided a significant benefit for the DSO, in such conditions, the network was able to accommodate over 80% adoption with voltages below 0.95 p.u. only 4.3% the time. A centralized PV-BESS system was incapable of ensure compliance with the standard EN50160 for adoptions above 20%, independently of the capacity of the system due to current limitations of the cabling, urging grid reinforcement prior its installation.

CRediT authorship contribution statement

Joel Alpízar-Castillo: Writing – review & editing, Writing – original draft, Visualization, Software, Methodology, Investigation, Formal analysis, Data curation, Conceptualization. **Laura Ramírez-Elizondo:** Validation, Supervision. **Arjan van Voorden:** Validation. **Pavol Bauer:** Validation, Funding acquisition.

Declaration of competing interest

The authors declare the following financial interests/personal relationships which may be considered as potential competing interests: Pavol Bauer reports financial support was provided by Netherlands Enterprise Agency. If there are other authors, they declare that they have no known competing financial interests or personal relationships that could have appeared to influence the work reported in this paper.

Acknowledgement

The project was carried out with a Top Sector Energy subsidy from the Ministry of Economic Affairs and Climate, carried out by the Netherlands Enterprise Agency (RVO). The specific subsidy for this project concerns the MOOI subsidy round 2020.

Data availability

The data that has been used is confidential.

References

[1] Electricity 2024: Analysis and forecast to 2026, Technical Report, International Energy Agency, 2024, URL: https://www.iea.org/reports/electricity-2024.
[2] Net Zero Roadmap: A Global Pathway to Keep the 1.5 ° C Goal in Reach, International Energy Agency, 2023, URL: https://www.iea.org/reports/space-heating.
[3] Global EV Outlook 2024, Technical Report, International Energy Agency, 2024, URL: https://www.iea.org/reports/global-ev-outlook-2024.
[4] Export Limitation, Application Note Version 2.8, SolarEdge, 2022, URL: https://knowledge-center.solaredge.com/sites/kc/files/feed-in_limitation_application_note.pdf.
[5] Technical Requirements for Customers' Export and Import Limitation Schemes, Engineering Recommendation G100 Issue 2 2022 Amendment 2, Energy Networks Association, 2023, URL: https://www.energynetworks.org/assets/images/ENA_EREC_G100_Issue_2_Amendment_2_(2023).pdf.
[6] D. Azuatalam, A.C. Chapman, G. Verbič, Probabilistic assessment of impact of flexible loads under network tariffs in low-voltage distribution networks, J. Mod. Power Syst. Clean Energy 9 (4) (2021) 951–962, http://dx.doi.org/10.35833/MPCE.2019.000136.
[7] 2030–2050 Integrated Infrastructure Outlook, Technical Report, Netbeheer Nederland, 2024, URL: https://www.energiekompas2050.nl/wp-content/uploads/2024/01/II3050-Main-Report-20240118-1.pdf.
[8] F. Norouzi, T. Hoppe, L.R. Elizondo, P. Bauer, A review of socio-technical barriers to smart microgrid development, Renew. Sustain. Energy Rev. 167 (2022) 112674, http://dx.doi.org/10.1016/j.rser.2022.112674, URL: https://www.sciencedirect.com/science/article/pii/S1364032122005640.
[9] G. Hovnanian, A. Kumar, R. Luby, Will a labor crunch derail plans to upgrade US infrastructure? 2022, URL: https://www.mckinsey.com/industries/public-sector/our-insights/will-a-labor-crunch-derail-plans-to-upgrade-us-infrastructure#/.
[10] J. Alpízar-Castillo, L. Ramirez-Elizondo, P. Bauer, Assessing the role of energy storage in multiple energy carriers toward providing ancillary services: A review, Energies 16 (1) (2023) http://dx.doi.org/10.3390/en16010379, URL: https://www.mdpi.com/1996-1073/16/1/379.
[11] T. Freire-Barceló, F. Martín-Martínez, Á. Sánchez-Miralles, A literature review of explicit demand flexibility providing energy services, Electr. Power Syst. Res. 209 (2022) 107953, http://dx.doi.org/10.1016/j.epsr.2022.107953, URL: https://www.sciencedirect.com/science/article/pii/S0378779622001833.
[12] D. Slaifstein, J. Alpízar-Castillo, A.M. Agudin, L. Ramírez-Elizondo, G.R.C. Mouli, P. Bauer, Aging-aware battery operation for multicarrier energy systems, in: IECON 2023- 49th Annual Conference of the IEEE Industrial Electronics Society, 2023, pp. 1–8, http://dx.doi.org/10.1109/IECON51785.2023.10312455.
[13] Y. Li, D.M. Vilathgamuwa, D.E. Quevedo, C.F. Lee, C. Zou, Ensemble nonlinear model predictive control for residential solar battery energy management, IEEE Trans. Control Syst. Technol. 31 (5) (2023) 2188–2200, http://dx.doi.org/10.1109/TCST.2023.3291540.
[14] M.M. Alam, M.H. Rahman, H. Nurcahyanto, Y.M. Jang, Energy management by scheduling ESS with active demand response in low voltage grid, in: 2020 International Conference on Information and Communication Technology Convergence, ICTC, 2020, pp. 683–686.
[15] W. Zou, J. Li, Q. Yang, Z. Duan, An improved max-min game theory control of fuel cell and battery hybrid energy system against system uncertainty, IEEE J. Emerg. Sel. Top. Power Electron. 11 (1) (2023) 78–87, http://dx.doi.org/10.1109/JESTPE.2022.3168374.

[16] P. Kurukuri, M.R. Mohamed, P.H. Raavi, Y. Arya, Optimal planning and designing of microgrid systems with hybrid renewable energy technologies for sustainable environment in cities, Env. Sci. Pollut. Res. Int. 31 (22) (2024) 32264–32281.

[17] M. Ahmed, A. Ganeshan, A.M. Amani, N. Al Khafaf, I.U. Nutkani, A. Vahidnia, M. Jalili, K. Hasan, M. Datta, R. Razzaghi, B. McGrath, L. Meegahapola, Effects of household battery systems on LV residential feeder voltage management, IEEE Trans. Power Deliv. 37 (6) (2022) 5325–5336, http://dx.doi.org/10.1109/TPWRD.2022.3176099.

[18] S.P. Menci, B. Herndler, F. Kupzog, M. Zweistra, R. Steegh, M. Willems, Scalability and replicability analysis of grid management services in low voltage networks in local flexibility markets: an InterFlex analysis, in: 2021 IEEE Madrid PowerTech, 2021, pp. 1–6, http://dx.doi.org/10.1109/PowerTech46648.2021.9495061.

[19] S. Ramírez-López, G. Gutiérrez-Alcaraz, M. Gough, M.S. Javadi, G.J. Osório, J.P.S. Catalão, Bi-level approach for flexibility provision by prosumers in distribution networks, IEEE Trans. Ind. Appl. 60 (2) (2024) 2491–2500, http://dx.doi.org/10.1109/TIA.2023.3330683.

[20] T. Gangwar, N.P. Padhy, P. Jena, Energy management approach to battery energy storage in unbalanced distribution networks, IEEE Trans. Ind. Appl. 60 (1) (2024) 1345–1356, http://dx.doi.org/10.1109/TIA.2023.3321030.

[21] K. Cao, Y. Liu, C. Wang, A distributionally robust optimal allocation method of energy storage for resilience enhancement of distribution network, in: 2023 IEEE International Conference on Energy Technologies for Future Grids, ETFG, 2023, pp. 1–6, http://dx.doi.org/10.1109/ETFG55873.2023.10407791.

[22] D. Jia, S. Wang, T. Kang, H. Yu, An optimal control strategy for LV distribution network with PV and energy storage units, in: 2022 7th International Conference on Power and Renewable Energy, ICPRE, 2022, pp. 1145–1150, http://dx.doi.org/10.1109/ICPRE55555.2022.9960574.

[23] G.M. Casolino, A. Losi, Flexibility aggregation perimeter for ancillary services in radial distribution systems, IEEE Access 11 (2023) 35945–35953, http://dx.doi.org/10.1109/ACCESS.2023.3265197.

[24] W. Li, X. Dou, Y. Shen, W. Hu, Voltage optimal strategy for low-voltage distribution network considering model missing, in: 2021 IEEE Sustainable Power and Energy Conference, ISPEC, 2021, pp. 2709–2713, http://dx.doi.org/10.1109/iSPEC53008.2021.9736062.

[25] V.M. Garrido-Arévalo, W. Gil-González, O.D. Montoya, L.F. Grisales-Noreña, J.C. Hernández, Optimal dispatch of DERs and battery-based ESS in distribution grids while considering reactive power capabilities and uncertainties: A second-order cone programming formulation, IEEE Access 12 (2024) 48497–48510, http://dx.doi.org/10.1109/ACCESS.2024.3382940.

[26] K. Hatipoglu, M. Olama, A new distributed model-free control strategy to diminish distribution system voltage violations, in: 2021 IEEE Power & Energy Society General Meeting, PESGM, 2021, pp. 1–5, http://dx.doi.org/10.1109/PESGM46819.2021.9638141.

[27] A.U. Rehman, J. Lu, B. Du, F. Bai, M.J. Sanjari, Efficient management of electric vehicle charging stations: Balancing user preferences and grid demands with energy storage systems and renewable energy, Appl. Energy 393 (2025) 126147, http://dx.doi.org/10.1016/j.apenergy.2025.126147, URL: https://www.sciencedirect.com/science/article/pii/S0306261925008773.

[28] S. Sarmokadam, M. Suresh, R. Mathew, Power flow control strategy for prosumer based EV charging scheme to minimize charging impact on distribution network, Energy Rep. 13 (2025) 3794–3809, http://dx.doi.org/10.1016/j.egyr.2025.03.032, URL: https://www.sciencedirect.com/science/article/pii/S2352484725001726.

[29] J. Alpízar-Castillo, L.M. Ramírez-Elizondo, P. Bauer, Modelling and evaluating different multi-carrier energy system configurations for a Dutch house, Appl. Energy 364 (2024) 123197, http://dx.doi.org/10.1016/j.apenergy.2024.123197.

[30] J. Wang, J. Purewal, P. Liu, J. Hicks-Garner, S. Soukazian, E. Sherman, A. Sorenson, L. Vu, H. Tataria, M.W. Verbrugge, Degradation of lithium ion batteries employing graphite negatives and nickel–cobalt–manganese oxide + spinel manganese oxide positives: Part 1, aging mechanisms and life estimation, J. Power Sources 269 (2014) 937–948, http://dx.doi.org/10.1016/j.jpowsour.2014.07.030, URL: https://linkinghub.elsevier.com/retrieve/pii/S037877531401074X, Empirical aging modelused by Wiljan.

[31] J. Alpízar-Castillo, A. Fu, L. Ramírez-Elizondo, M. Cvetkovic, P. Bauer, Multi-carrier energy home energy management system using genetic algorithms and random forest predictions, in: 2024 IEEE Energy Conversion Congress and Exposition, ECCE, 2024, pp. 1037–1044, http://dx.doi.org/10.1109/ECCE55643.2024.10861342.

[32] S. Bolognani, S. Zampieri, On the existence and linear approximation of the power flow solution in power distribution networks, IEEE Trans. Power Syst. 31 (1) (2016) 163–172, http://dx.doi.org/10.1109/TPWRS.2015.2395452.

[33] J. Alpízar-Castillo, L. Ramírez-Elizondo, P. Bauer, The effect of non-coordinated heating electrification alternatives on a low-voltage distribution network with high PV penetration, in: 2023 IEEE 17th International Conference on Compatibility, Power Electronics and Power Engineering, CPE-POWERENG, 2023, pp. 1–6, http://dx.doi.org/10.1109/CPE-POWERENG58103.2023.10227394, URL: https://ieeexplore.ieee.org/document/10227394.

[34] J. Alpízar-Castillo, L. Ramírez-Elizondo, P. Bauer, Addressing premature reinforcement of low-voltage distribution infrastructure with peak-shaving and power curtailment: a business model, in: 2024 20th International Conference on the European Energy Market, EEM, 2024, pp. 1–6.

[35] J. Alpízar-Castillo, K. Linders, D. Slaifstein, L. Ramírez-Elizondo, P. Bauer, Economic opportunities of power curtailment and peak shaving on residential PV-BESS systems, in: 2024 20th International Conference on the European Energy Market, EEM, 2024, pp. 1–6, http://dx.doi.org/10.1109/EEM60825.2024.10608921.